91602
new 82-10

ontario hydro
research division

COMPLIMENTARY COPY
Please Credit Ontario Hydro Research if
Reproduced in Whole or in Part

Standstill Frequency Response Test
Atikokan TGS

Report No 87-266-K

J.R.R. Service
Engineer
System Studies Section

ABSTRACT

Ontario Hydro conducted a standstill frequency response (SSFR) test on the generator manufactured by Brown-Boveri Company at Atikokan TGS. Testing was done in accordance with IEEE standard 115A-1987 [2]. Using a least-squares iterative technique, direct and quadrature axis equivalent circuits were fitted to the SSFR data. An unusual aspect of the Atikokan rotor (from Ontario Hydro's perspective) is the presence of a "squirrel-cage" damper winding. The effects of this winding are illustrated by the absence of the first amortisseur circuit inductance, L_{1d}, and the presence of a differential leakage element, L_{f1d}, in the "best-fit" direct axis equivalent circuit. Fitting errors of the various equivalent circuit models with respect to the SSFR data are discussed. Appendix A tabulates and shows plots of the SSFR test data.

job	file	date	report no.
18-173-421	813.11	November 23, 1987	87-266-K

Table of Contents

STANDSTILL FREQUENCY RESPONSE TEST - ATIKOKAN TGS	1
INTRODUCTION	1
MEASUREMENTS	2
BASE VALUES FOR THE DATA ANALYSIS	3
DIRECT AXIS	4
Operational Inductance	4
Turn Ratio	4
Operational Field Resistance	5
Equivalent Circuit Model Nomenclature	5
Equivalent Circuit Models	6
Adjustment to Unsaturated Conditions	7
Field Resistance	8
Normalized Models	9
Other Per-Unit Bases	11
QUADRATURE AXIS	11
COMMENTS ON EQUIVALENT CIRCUITS	15
CONCLUSION	18
ACKNOWLEDGMENTS	18
REFERENCES	19

Appendices

A:	STANDSTILL FREQUENCY RESPONSE TEST DATA - ATIKOKAN TGS	A-1

List of Figures

1:	Equipment Arrangement for Standstill Frequency Response Testing	3
2:	Direct Axis Equivalent Circuit Models: Df21, Df11 and Df10	6
3:	Open Circuit Saturation Curve for the Atikokan Generator	8
4:	Recommended Direct Axis Equivalent Circuit Models: $Df21_{Q3}$, $Df11_{Q2}$ and $Df10_{Q2}$	10
5:	Quadrature Axis Equivalent Circuit Models	12

Table of Contents

List of Figures

6:	Recommended Quadrature Axis Equivalent Circuit Models: $Q3_{Df21}$, Model $Q2_{Df11}$ and $Q2_{Df10}$	14
7:	Weighting Factors vs. Frequency for Standstill Frequency Response Fitting	16
8:	"Best Fit" Equivalent Circuit Models: Df22 and Q3	17
9:	Low Frequency Direct Axis, Field Shorted, Impedance, $Z_d(s) = R_d(s) + jX_d(s)$ Resistance, $R_d(s)$ and Reactance, $X_d(s)$ vs. Frequency	20
10:	Field Current to Direct Axis Stator Current Transfer Function, $\Delta I_{fd}(s)/\Delta I_d(s)$ Magnitude vs. Low Frequency	21
11:	Field Voltage to Direct Axis Stator Current Transfer Function, $\Delta E_{fd}(s)/\Delta I_d(s)$ Magnitude vs. Low Frequency	21
12:	Comparison of SSFR Data with the Equivalent Circuit Models Responses for the Direct Axis, Field Shorted, Operational Inductance Under Standstill Test Conditions	22
13:	Comparison of SSFR Data with the Equivalent Circuit Models Responses for the Field Current to Direct Axis Stator Current Transfer Function Under Standstill Test Conditions	23
14:	Low Frequency Quadrature Axis Impedance, $Z_q(s)$ Resistance, $R_q(s)$ and Reactance, $X_q(s)$ vs. Frequency	24
15:	Comparison of SSFR Data with the Equivalent Circuit Models Responses for the Quadrature Axis Operational Inductance Under Standstill Test Conditions	25
A-1:	Direct Axis Impedance, Field Shorted, $Z_d(s)$ Magnitude and Phase vs. Frequency	A-4
A-2:	Direct Axis Operational Inductance, Field Shorted, $L_d(s)$ Magnitude and Phase vs. Frequency	A-5
A-3:	Field Current to Direct Axis Stator Current Transfer Function, $\Delta I_{fd}(s)/\Delta I_d(s)$ Magnitude and Phase vs. Frequency	A-6
A-4:	Direct Axis Impedance, Field Open, $Z_{do}(s)$ Magnitude and Phase vs. Frequency	A-9
A-5:	Low Frequency Direct Axis, Field Open, Impedance Resistance, $R_{do}(s)$ and Reactance, $X_{do}(s)$ vs. Frequency	A-10

Table of Contents

List of Figures

A-6:	Direct Axis Operational Inductance, Field Open, $L_{do}(s)$ Magnitude and Phase vs. Frequency	A-11
A-7:	Field Voltage to Direct Axis Stator Current Transfer Function, $\Delta E_{fd}(s)/\Delta I_d(s)$ Magnitude and Phase vs. Frequency	A-12
A-8:	Quadrature Axis Impedance, $Z_q(s)$, Magnitude and Phase vs. Frequency	A-15
A-9:	Quadrature Axis Operational Inductance, $L_q(s)$ Magnitude and Phase vs. Frequency	A-16
A-10:	Field Impedance, Stator Open, $Z_{fdo}(s)$, Magnitude and Phase vs. Frequency	A-19

List of Tables

1:	Direct Axis Equivalent Circuit Parameter Values	7
2:	Per-Unit Unsaturated Equivalent Circuit Model Parameter Values for the Direct Axis	9
3:	Quadrature Axis Equivalent Circuit Parameter Values	13
4:	Per-Unit Unsaturated Equivalent Circuit Model Parameter Values for the Quadrature Axis	14
5:	Comparison of Equivalent Circuit Model Errors With Respect to the Standstill Frequency Response Data	17
A-1:	Direct Axis, Field Shorted, Test Data	A-2
A-2:	Direct Axis, Field Open, Test Data	A-7
A-3:	Quadrature Axis, Test Data	A-13
A-4:	Field Impedance, Stator Open, Test Data	A-17

To Mr. Z. J. Janik
Manager - Op. Eng. & Pgm Mgmt
Design & Development - Generation

ontario hydro
research division

STANDSTILL FREQUENCY RESPONSE TEST - ATIKOKAN TGS

INTRODUCTION

Synchronous machine parameters may be derived from the data measured with the standstill frequency response (SSFR) test described in IEEE standard 115A-1987 [2]. Part 3 of EPRI report EL-1424 [3] explains the theoretical basis for the SSFR test. In summary, a variable frequency source injects a current into two of three phases of the stator winding. The measurements are first performed with the magnetic axis of the field circuit aligned with the two phases, ie, the direct axis. The frequency response is measured both with the field open and with the field shorted. Next, after aligning the field winding magnetic axis at right angles to the two stator phases, the quadrature axis, another set of frequency response measurements is taken. Ontario Hydro carried out the test on the generator at Atikokan in February, 1985. This machine of Brown-Boveri Company - Baden (BBC) manufacture has a rating of 270 MVA, 0.85 power factor and a terminal voltage of 18 kV.

Construction of the rotor in the Atikokan unit differs from all the other large turbo-generators owned by Ontario Hydro (except for the Darlington units also manufactured by BBC). The unusual feature of the rotor is that it is surrounded with a complete damper winding cage. As a result the current flow in the rotor is split among the field and damper windings, the rotor body and, possibly, in the field slot wedges (At standstill, slot wedge conduction is probably small because the cumulative contact resistances of the short wedges would be large.). Now, without a discrete damper winding, the field self inductance, L_{ffd}, is the sum of the direct axis mutual inductance, L_{ad}, and the field leakage inductance, L_{fd}. The direct axis amortisseur impedance, $Z_{f1d} = R_{f1d} + j(\omega/\omega_o)L_{f1d}$ (see Figure 2), represents rotor-body effects. In the case of Atikokan, however, the damper winding would be expected to introduce an additional differential leakage term, L_{f1d}, into $L_{ffd} = L_{ad} + L_{f1d} + L_{fd}$. Thus, the field leakage inductance, L_{fd}, would be smaller because of the split current paths between the two windings. The first amortisseur impedance would become a simple resistance, $Z_{f1d} = R_{f1d}$. These effects came out clearly during the equivalent circuit fitting process (Figure 4, models $Df21_{Q3}$ and $Df11_{Q2}$).

MEASUREMENTS

The standstill generator frequency response was measured over a frequency range of 0.001 to 1000 Hz. Test points were logarithmically spaced at 10 points per decade in the range 0.01 to 1000 Hz and 40 points per decade in the decade 0.001 to 0.01 Hz. In order to measure the DC stator resistance as accurately as possible under standstill test conditions this higher resolution is required in the very low frequency decade. The following functions were measured on the Atikokan generator:

$\frac{\Delta E_{Sd}}{\Delta I_{Sd}}$, $\frac{\Delta I_{fd}}{\Delta I_{Sd}}$	Rotor in direct axis position with the field shorted
$\frac{\Delta E_{Sdo}}{\Delta I_{Sdo}}$, $\frac{\Delta E_{fd}}{\Delta I_{Sdo}}$	Rotor in direct axis position with the field open
$\frac{\Delta E_{Sq}}{\Delta I_{Sq}}$	Rotor in quadrature axis position
$\frac{\Delta E_{fdo}}{\Delta I_{fdo}}$	Stator open

Three power amplifiers, with a combined capability of 20 V, 60 A peak, supplied the test current as is shown in Figure 1. Using a computer-controlled setup permits the frequency response analyzer generating a sinusoidal reference output to be adjusted to produce as much current as possible at each frequency and to automatically store the results. In the Appendix A the measured data are plotted and tabulated.

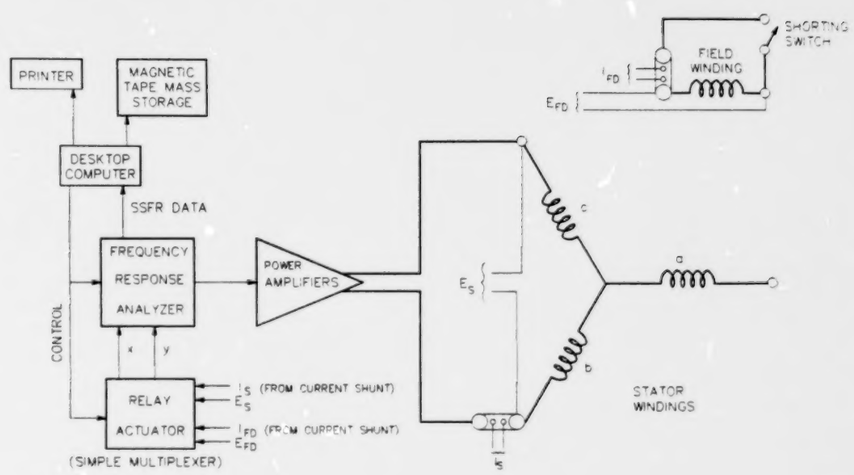

Figure 1: Equipment Arrangement for Standstill Frequency Response Testing

BASE VALUES FOR THE DATA ANALYSIS

The rating of this BBC machine is 270 MVA, power factor of 0.85 and rated terminal voltage of 18 kV. The base impedance is calculated as follows:

$$Z_{base} = \frac{(\text{Rated } E_t \text{ in kV})^2}{\text{Rated MVA}}$$

$$= \frac{18^2}{270}$$

$$= 1.2\,\Omega$$

And the base inductance is derived as shown below:

$$L_{base} = \frac{Z_{base}}{\omega_0}$$

$$= \frac{1.2}{(2\pi)60}$$

$$= 3.183 \text{ mH}$$

The manufacterer's calculated value for the stator leakage inductance, L_ℓ, is 0.16 pu or 0.509 mH. This inductance is common to both the direct and quadrature axes.

DIRECT AXIS

Operational Inductance

Let $Z_d(s) = \frac{1}{2}\frac{E_{Sd}(s)}{I_{Sd}(s)}$ for the test setup shown in Figure 1 with the magnetic axis of the field winding aligned with the direct axis of the stator. The direct axis stator resistance, R_{ad}, will be defined as

$$R_{ad} = \lim_{s \to 0} Z_d(s) .$$

A plot in rectangular co-ordinates of the impedance, $Z_d(s) = R_d(s) + jX_d(s)$, measured at the stator terminals with the field shorted is shown in Figure 9. From the low frequency asymptote of $R_d(s)$ in Figure 9, R_{ad} was found to be:

$$R_{ad} = 0.84\ m\Omega.$$

This asymptote was obtained by fitting a function $R_{ad} \cdot (1 + K[2\pi f]^2)$ for $f < 10^{-2}$ Hz to the $R_d(s)$ data plotted in Figure 9. $L_d(0)$ is defined as the "low frequency" slope of the line passing through the origin and the $X_d(s)$ data points and was found to be equal to 5.435 mH. The value of L_{adSS}, the direct axis stator to rotor mutual inductance under standstill test conditions of saturation, is calculated as shown below:

$$\begin{aligned} L_{adSS} &= L_d(0) - L_\ell \\ &= 5.435 - 0.509 \\ &= 4.926\ mH. \end{aligned}$$

$L_d(s)$, the direct axis, field shorted, operational inductance is calculated from the following expression:

$$L_d(s) = \frac{Z_d(s) - R_{ad}}{s}.$$

A plot of this function derived from the measured Atikokan data is shown in Figure 13.

Turn Ratio

The field to stator turn ratio, N_{fd}/N_a, is derived from the low frequency decade/decade asymptote

to the transfer function $\Delta E_{fd}(s)/\Delta I_d(s)$ plotted in Figure 11.

$$\frac{N_{fd}}{N_a} = \frac{1}{L_{adSS}} \lim_{s\to 0} \left[\frac{1}{s} \frac{\Delta E_{fd}(s)}{\Delta I_d(s)} \right] \quad \text{where} \quad \frac{\Delta E_{fd}(s)}{\Delta I_d(s)} = \frac{\sqrt{3}}{2} \frac{\Delta E_{fd}}{\Delta I_{Sdo}}$$

$$= \frac{0.06415}{0.004926}$$

$$= 13.02$$

Operational Field Resistance

The field resistance referred to the stator is found from the low frequency decade/decade asymptote to the transfer function $\Delta I_{fd}(s)/\Delta I_d(s)$ in Figure 10.

$$R_{fd} = \frac{L_{adSS}}{\lim_{s\to 0} \left[\frac{1}{s} \frac{\Delta I_{fd}(s)}{\Delta I_d(s)} \right] \frac{2}{3} \left(\frac{N_{fd}}{N_a}\right)} \quad \text{where} \quad \frac{\Delta I_{fd}(s)}{\Delta I_d(s)} = \frac{\sqrt{3}}{2} \frac{\Delta I_{fd}}{\Delta I_{Sd}}$$

$$= \frac{0.004926}{(0.4580)\ (\frac{2}{3})\ (13.02)}$$

$$= 0.999\ m\Omega$$

This value of R_{fd} is the combined resistance, referred to the stator, of the field winding, the metering shunt and connecting leads, all in the circuit during the frequency response measurement of $\Delta I_{fd}/\Delta I_{Sd}$.

Equivalent Circuit Model Nomenclature

The following nomenclature has been adopted for the equivalent circuit models shown in Figure 2:

Symbol	Meaning
D	direct axis model
Q	quadrature axis model
f	field circuit (L_{fd} and R_{fd})
first digit	number of amortisseur circuits (eg L_{1d} & R_{1d}, L_{2d} & R_{2d} or L_{1q} & R_{1q}, L_{2q} & R_{2q}, L_{3q} & R_{3q})
second digit	number of differential leakage inductances (eg L_{f12d} or L_{f1d}, L_{f2d})

For example, Df21 would represent a direct axis equivalent circuit model with a field winding, two amortisseur windings and one differential leakage inductance element. Certain direct and quadrature axis models may have some common parameter during the parameter-fitting process (such as when the sub-sub-transient reactances are forced to be equal). This commonality is indicated either by a subscript or brackets around the appropriate model in the other axis. For example, the models $Df21_{Q3}$ and $Q3_{Df21}$ or, alternatively, Df21(Q3) and Q3(Df21) are a related model set with equal sub-sub-transient reactance magnitudes.

Equivalent Circuit Models

In Figure 2 are shown the equivalent circuit models fitted to the $L_d(s)$ and $\Delta I_{fd}(s)/\Delta I_d(s)$ direct axis transfer functions. Only these two transfer functions were used for the direct axis because they reflect the normal operating condition of the generator. The two direct axis transfer functions, $Z_{do}(s)$ and $\Delta E_{fd}(s)/\Delta I_d(s)$, measured with the field open, represent an abnormal operating condition. However, the turn ratio is obtained from the latter function as was shown on page 4 . The operational inductance, $L_{do}(s)$, can be derived from the $Z_{do}(s)$ measurements shown in Figure A-5 and values for R_{ado} and $L_{do}(0)$ can be obtained to cross-check the values derived form the direct axis data with the field shorted.

Table 1 shows the model parameters obtained using a least squares iterative parameter fitting technique. Note also that the high frequency asymptotes of the $L_d(s)$ and $L_q(s)$ functions for the models $Df21_{Q3}$, $Df11_{Q2}$ and $Df1_{Q2}$ were constrained to be equal. For system stability computer programs using direct and quadrature axis models with sub-(sub-)transient saliency is more convenient.

Figure 2: Direct Axis Equivalent Circuit Models: Df21, Df11 and Df10

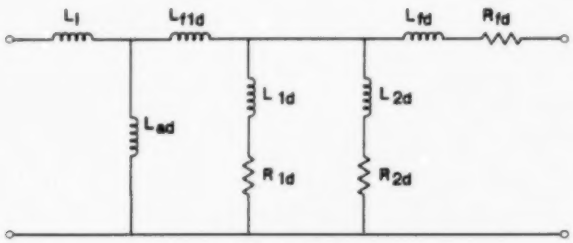

Model Df21

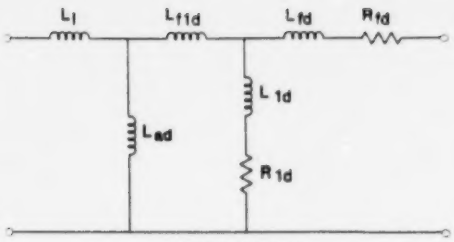

Model Df11

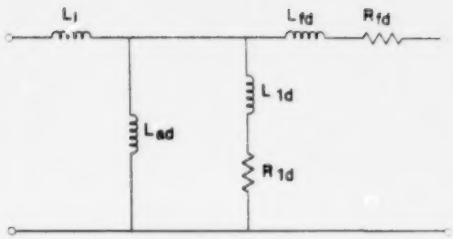

Model Df10

Table 1: Direct Axis Equivalent Circuit Parameter Values

Parameter	Model $Df21_{Q3}$ (L'''_d=L'''_q)	Model $Df11_{Q2}$ (L''_d=L''_q)	Model $Df1_{Q2}$ (L''_d=L''_q)	Units
L_ℓ	0.509	0.509	0.509	mH
L_{adSSFR}	4.926	4.926	4.926	mH
$L_{f1(2)d}$	0.08554	0.2202	n/a	mH
L_{1d}	0.0	0.0	0.0	mH
R_{1d}	10.40	6.122	13.30	mΩ
L_{f2d}	n/a	n/a	n/a	mH
L_{2d}	6.818	n/a	n/a	mH
R_{2d}	4.914	n/a	n/a	mΩ
L_{fd}	0.2853	0.1589	0.3689	mH
R_{fd}	0.9986	0.9986	0.9986	mΩ @ 19.9 °C

n/a - not applicable

The operational inductance, $L_d(s)$, and the field current to stator current transfer function, $\Delta E_{fd}(s)/\Delta I_d(s)$, calculated with these model parameter values are plotted with the corresponding test data in Figures 12 and 13.

Adjustment to Unsaturated Conditions

At this point, the generator model is valid for the flux levels at which the standstill frequency response was done. These low flux levels result in iron dependent inductances which are lower in value than they would be under the unsaturated conditions defined by the air gap line of the open circuit saturation curve shown in Figure 3 [8]. Assuming L_{ad} is the only iron-dependent inductance in the direct axis equivalent circuit, the models can be adjusted to unsaturated conditions in the following manner. At rated stator voltage on the air gap line the field current is

775 A. The unsaturated value of the field to stator mutual inductance is:

$$L_{aduOCS} = \frac{3}{2}\left[\frac{N_a}{N_{fd}}\right]\frac{E_{t\text{-}pk\text{-}ln}}{\omega_0 I_{fd}} \qquad \text{(Peak line-to-neutral terminal voltage)}$$

where $E_{t\text{-}pk\text{-}ln}/I_{fd}$ is the slope of the air gap line and ω_0 is $2\pi 60$ electrical radians/second. Substituting the values for the Atikokan machine gives the following value for L_{adOCS}:

$$L_{aduOCS} = \frac{3}{2}\left(\frac{1}{12.01}\right)\frac{18000\sqrt{\frac{2}{3}}}{(2\pi 60)(775)}$$

$$= 5.795 \text{ mH}$$

$$= 1.821 \text{ pu}$$

L_{adOCS} will be substituted for the value of L_{adSS} used previously to fit the models to the SSFR data.

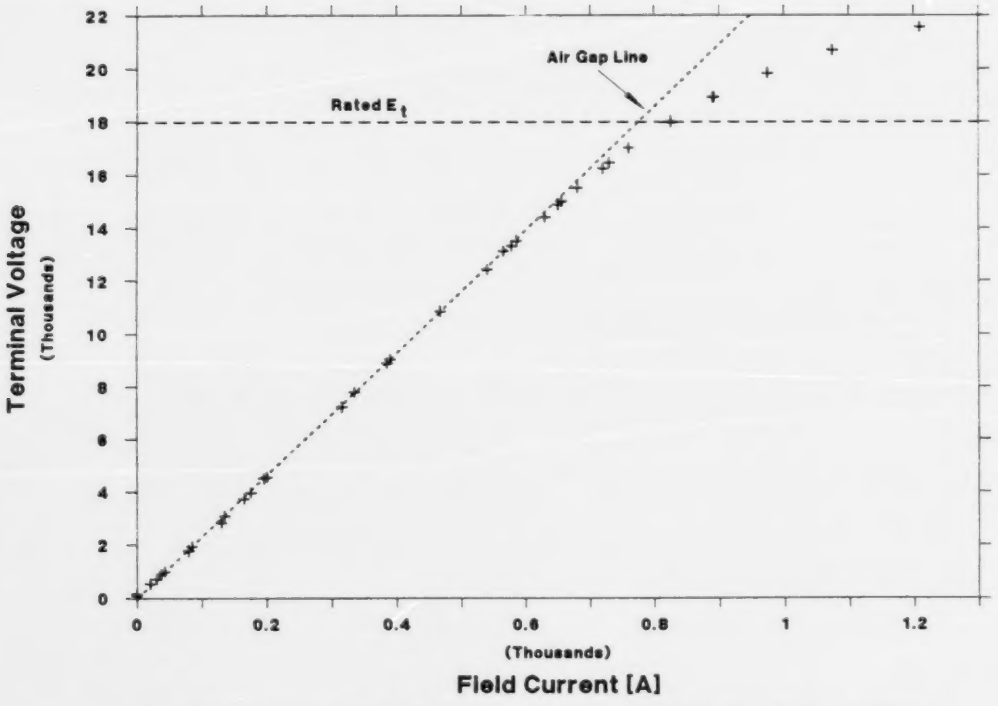

Figure 3: Open Circuit Saturation Curve for the Atikokan Generator

Field Resistance

The field winding resistance, r_{fd}, measured during the standstill test was 0.1082 at 19.9 °C. Refer this resistance to the stator at the "standard" rotor operating temperature of 100 °C, using the

following expression [5]:

$$R_{fd} = \left(\frac{T_c + T_{op}}{T_c + T_a} \right) (r_{fd}) \left(\frac{3}{2}\right) \left(\frac{N_a}{N_{fd}} \right)^2$$

where T_c is the temperature coefficient of resistivity of copper.

$$= \left(\frac{234.5 + 100}{234.5 + 19.9} \right) (0.1082) \left(\frac{3}{2}\right) \left(\frac{1}{13.02} \right)^2$$

$$= 1.259 \text{ m}\Omega$$

$$= 0.001049 \text{ pu}$$

Normalized Models

Table 2 shows the parameter values converted to per unit on the machine rating and Figure 4 depicts the recommended direct axis equivalent circuit models with these values.

Table 2: Per-Unit Unsaturated Equivalent Circuit Model Parameter Values for the Direct Axis

Parameter	Model $Df21_{Q3}$ (L'''_d=L'''_q)	Model $Df11_{Q2}$ (L''_d=L'_q)	Model $Df1_{Q2}$ (L''_d=L''_q)
L_ℓ	0.1599	0.1599	0.1599
L_{adOCS}	1.821	1.821	1.821
$L_{f1(2)d}$	0.02687	0.06918	n/a
L_{1d}	0.0	0.0	0.0
R_{1d}	0.008667	0.005102	0.01108
L_{f2d}	n/a	n/a	n/a
L_{2d}	2.142	n/a	n/a
R_{2d}	0.004095	n/a	n/a
L_{fd}	0.08963	0.04992	0.1159
R_{fd}	0.001049	0.001049	0.001049 @ 100 °C

n/a - not applicable Bases: 270 MVA, 18 kV

Figure 4: Recommended Direct Axis Equivalent Circuit Models:

$Df21_{Q3}$, $Df11_{Q2}$ and $Df10_{Q2}$

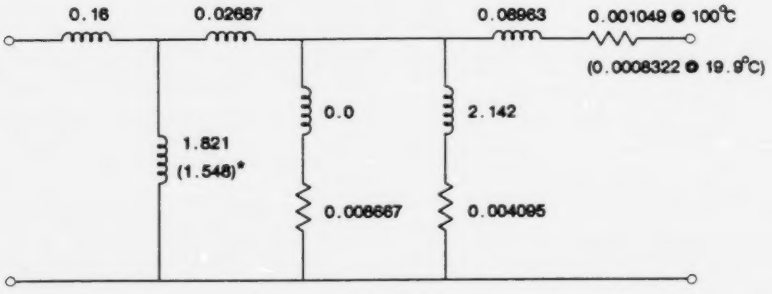

Model $Df21_{Q3}$

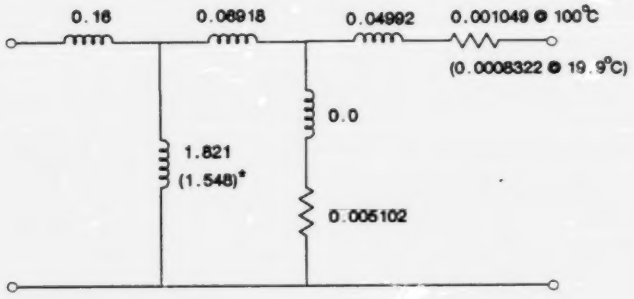

Model $Df11_{Q2}$

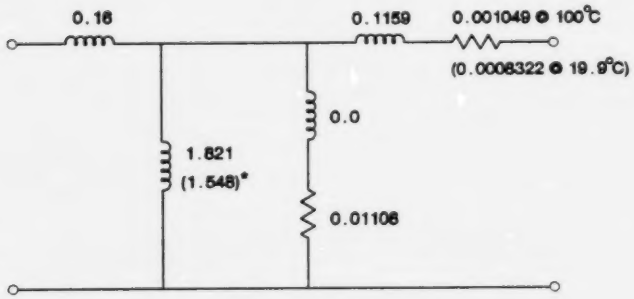

Model $Df10_{Q2}$

Per-Unit Bases: 270 MVA, 18 kV

* value of L_{ad} under standstill test saturation conditions

Other Per-Unit Bases

The stator current base is calculated by the following expression:

$$I_{Sbase} = \frac{\text{Rated MVA} \times 10^6}{\sqrt{3} \cdot \text{Rated } E_{t(l\text{-}l)}}$$

$$= \frac{270 \times 10^6}{\sqrt{3} \cdot 18000}$$

$$= 8.660 \text{ kA}$$

The field current base is defined by Rankin [4] as shown below:

$$I_{fd\text{-}base} = \left[\frac{3}{2}\right] \left(\frac{N_a}{N_{fd}}\right) (I_{Sbase\text{-}peak})$$

$$= \left[\frac{3}{2}\right] \left(\frac{1}{13.02}\right) (8660)$$

$$= 1.411 \text{ kA}$$

Calculate the field impedance base at 100 °C as shown below:

$$Z_{fd\text{-}base} = \frac{\text{Rated MVA} \times 10^6}{I^2_{fd\text{-}base}}$$

$$= \frac{270 \times 10^6}{(1411)^2}$$

$$= 135.6 \ \Omega$$

At 100°C the field resistance referred to the field is calculated by the expression shown below:

$$R_{fd} = \left(\frac{T_c + T_{op}}{T_c + T_a} \right) (r_{fd})$$

$$= \left(\frac{234.5 + 100}{234.5 + 19.9} \right) (0.1082)$$

$$= 0.1423 \ \Omega$$

$$= 0.001049 \text{ pu}$$

QUADRATURE AXIS

The analysis for the quadrature axis proceeds in a similar fashion to that of the direct axis;

however, there is no field circuit. From Figure 14 the low frequency asymptote of $R_q(s)$ is:

$$R_{aq} = \lim_{s \to 0} Z_q(s)$$
$$= 0.84\ m\Omega$$

The low frequency limit $L_q(0)$ is found from the slope of the line going through the origin along the curve of $X_q(s)$ shown in Figure 14.

$$L_q(0) = 5.436\ mH$$

L_{aqSS}, the quadrature axis mutual inductance, under standstill test conditions is calculated by the expression shown:

$$L_{aqSS} = L_q(s) - L_\ell$$
$$= 5.436 - 0.509$$
$$= 4.927\ mH$$

In Figure 15 is plotted the quadrature operational inductance calculated from the impedance data shown in Figure A-8 using the expression shown below:

$$L_q(s) = \frac{Z_q(s) - R_{aq}}{s}$$

where $Z_q(s) = \frac{1}{2} \frac{\Delta E_{Sq}(s)}{\Delta I_{Sq}(s)}$.

The two equivalent circuit models shown in Figure 5 were fitted to the operational inductance curve derived from the standstill frequency response data using a least-squares pattern-search iterative technique [4]. The models' responses under standstill test conditions are plotted in Figure 15. The models' parameter values are shown in Table 3.

Figure 5: Quadrature Axis Equivalent Circuit Models

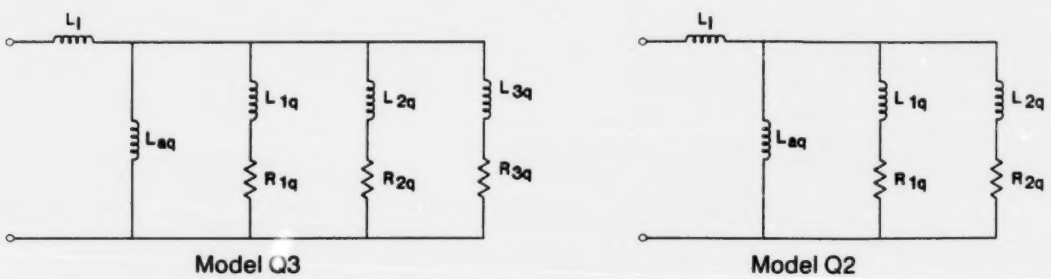

Table 3: Quadrature Axis Equivalent Circuit Parameter Values

Parameter	Model $Q3_{Df21}$ ($L'''_q=L'''_d$)	Model $Q2_{Df11}$ ($L''_q=L''_d$)	Model $Q2_{Df1}$ ($L''_q=L''_d$)	Units
L_ℓ	0.509	0.509	0.509	mH
L_{aqSSFR}	4.927	4.927	4.927	mH
L_{1q}	0.935	0.2600	0.0	mH
R_{1q}	15.52	33.94	46.23	mΩ
L_{2q}	3.240	1.436	1.244	mH
R_{2q}	5.209	6.702	6.988	mΩ
L_{3q}	0.09630	n/a	n/a	mH
R_{3q}	117.1	n/a	n/a	mΩ

n/a - not applicable

Assume that the saturation under standstill test conditions in the quadrature axis has the same ratio as in the direct axis:

$$L_{aqu} = L_{aqSSFR} \frac{L_{adOCS}}{L_{adSSFR}}$$

$$= 4.927 \frac{5.795}{4.926}$$

$$= 4.927 \cdot 1.176$$

$$= 5.796 \text{ mH}$$

$$= 1.821 \text{ pu}$$

Table 4 lists the per unit, unsaturated, quadrature axis equivalent circuit parameter values on the machine basis. Figure 6 shows the recommended quadrature axis models.

Table 4: Per-Unit Unsaturated Equivalent Circuit Model Parameter Values for the Quadrature Axis

Parameter	Model $Q3_{Df21}$ ($L'''_q = L'''_d$)	Model $Q2_{Df11}$ ($L''_q = L''_d$)	Model $Q2_{Df1}$ ($L''_q = L''_d$)
L_ℓ	0.1599	0.1599	0.1599
L_{aqu}	1.821	1.821	1.821
L_{1q}	0.2937	0.08168	0.0
R_{1q}	0.01293	0.02828	0.03853
L_{2q}	1.018	0.4511	0.3908
R_{2q}	0.004341	0.005585	0.005823
L_{3q}	0.03025	n/a	n/a
R_{3q}	0.09758	n/a	n/a

n/a - not applicable Bases: 270 MVA, 18 kV

Figure 6: Recommended Quadrature Axis Equivalent Circuit Models: $Q3_{Df21}$, Model $Q2_{Df11}$ and $Q2_{Df10}$

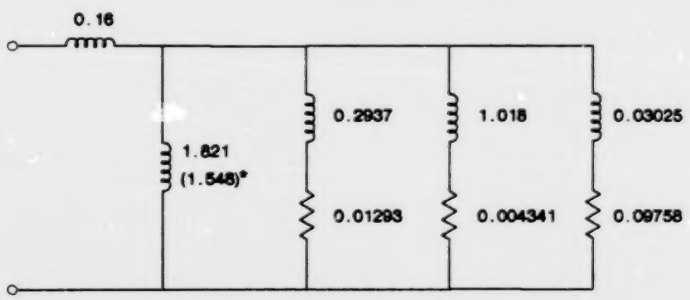

Model $Q3_{Df21}$

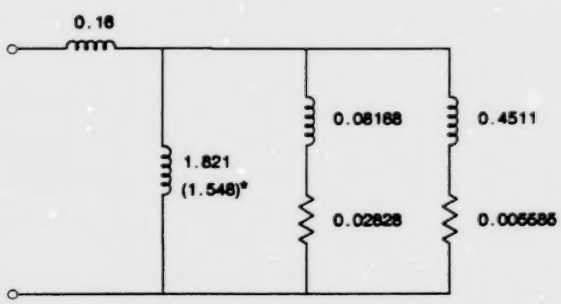

Model $Q2_{Df11}$

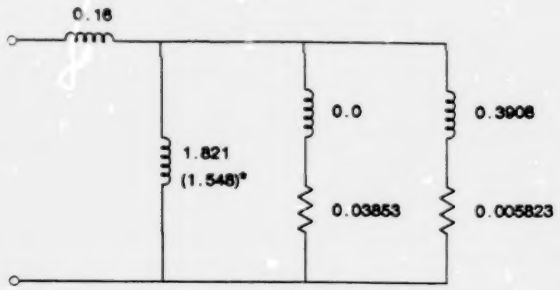

Model $Q2_{Df10}$

Per-Unit Bases: 270 MVA, 18 kV

* value of L_{aq} under standstill test saturation conditions

COMMENTS ON EQUIVALENT CIRCUITS

The high frequency asymptotes (ie, the sub-sub or subtransient region depending on the equivalent circuit model order) of the direct and quadrature axis operational inductances were forced to be equal. This was done for computational convenience in system stability programs which use these models.

As has been mentioned these models were fitted using a least-squares pattern-search iterative approach. The test data had various weightings over different frequency ranges as shown in Figure 7. The "fixed" values (ie, L_{ad}, L_{aq}, R_{fd} and N_{fd}/N_a) were obtained graphically by fitting simple curves to the low frequency response data. Thus, these parameters have already been "fitted" to the low frequency standstill test data and this frequency range of data may be omitted from the fitting of the remainder of the unknown equivalent circuit parameters. The high frequency range (>300 Hz) of test data was ignored because of the increased measurement error resulting from the higher impedances which prevent the power amplifiers from maintaining as high a flux level as for the lower frequencies.

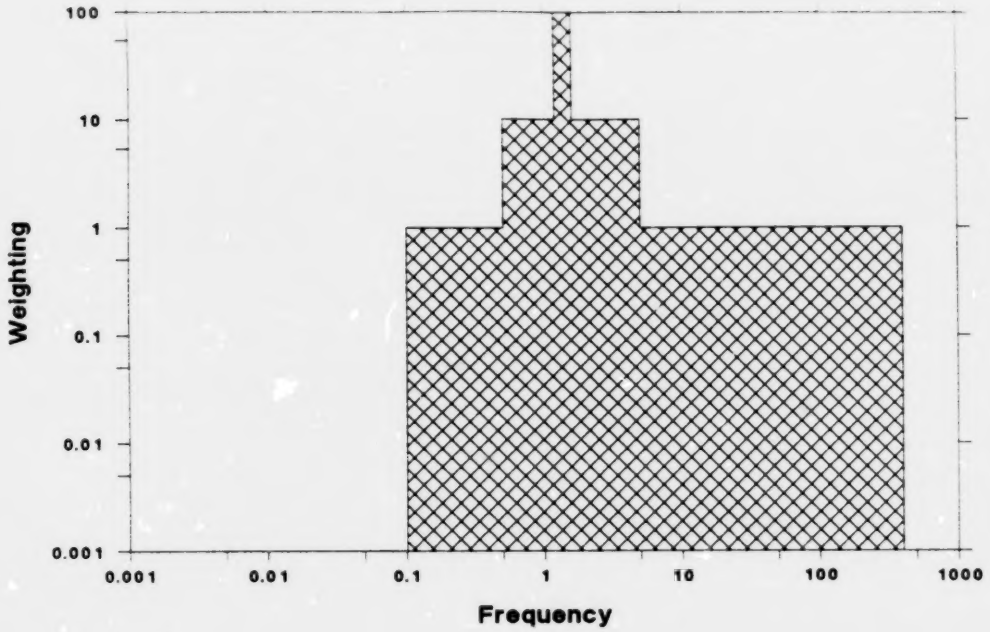

Figure 7: Weighting Factors vs. Frequency for Standstill Frequency Response Fitting

The weightings for each standstill frequency reponse measurement function are shown below:

Direct Axis Operational Inductance, Field Shorted, $L_d(s)$	2
Field Current to Direct Axis Stator Current Transfer Function	1
Quadrature Axis Operational Inductance, $L_q(s)$	2

The various equivalent circuit models can be compared with the actual measured SSFR data by normalizing the fitting error with respect to the "best fit" models Df22 and Q3. The parameters of these two models are shown in Figure 8.

Figure 8: "Best Fit" Equivalent Circuit Models: Df22 and Q3

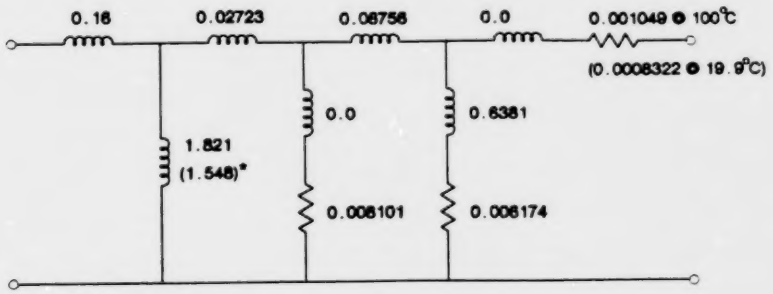

Model Df22

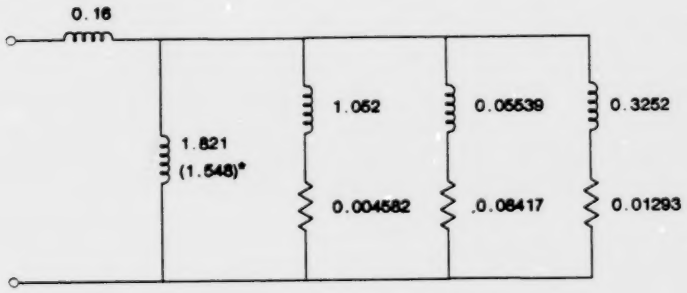

Model Q3

Per-Unit Bases: 270 MVA, 18 kV

* values under standstill test saturation conditions

Table 5: Comparison of Equivalent Circuit Model Errors With Respect to the Standstill Frequency Response Data

Model	Normalized Error
Df22 and Q3 fitted to SSFR Data	1.00
$Df22_{Q3}$ and $Q3_{Df22}$ fitted to SSFR Data and $L_d(\infty) \simeq L_q(\infty)$	1.02
Df21 and Q3 fitted to SSFR Data	1.02
$Df21_{Q3}$ and $Q3_{Df21}$ fitted to SSFR Data and $L_d(\infty) \simeq L_q(\infty)$	1.03
Df11 and Q2 fitted to SSFR Data	1.22
$Df11_{Q2}$ and $Q2_{Df11}$ fitted to SSFR Data and $L_d(\infty) \simeq L_q(\infty)$	1.37
Df10 and Q2 fitted to SSFR Data	1.39
$Df10_{Q2}$ and $Q2_{Df10}$ fitted to SSFR Data and $L_d(\infty) \simeq L_q(\infty)$	1.54

The Atikokan rotor design includes a complete squirrel cage damper winding as was explained

in the Introduction. This shows up in the fitted models by the disappearance of L_{1d} and the non-zero value of differential leakage inductance, L_{f1d}. Table 5, comparing the model response errors with respect to the measured standstill test data, and the curves plotted in Figures 12, 13 and 15, illustrate this. Omitting one differential leakage inductance, L_{f2d}, only slightly increases the error value. Forcing sub-sub- (or sub-) transient saliency to be equal in the direct and quadrature axes does not make a significant difference in the error for the Df2x and Q3 models. However, using a reduced order model with fewer elements in the equivalent circuit to adjust for a fit to the frequency response data increases the error by a relatively larger amount for the Df1x and Q2 models. The fitting error of the direct axis model, with a differential leakage inductance fixed at zero, is larger still.

CONCLUSION

Complete direct and quadrature axes equivalent circuit models have been fitted solely to the standstill frequency response test data measured on the Atikokan generator. The equivalent circuit models: $Df21_{Q3}$ and $Q3_{Df21}$ correspond to model 3.3 of Reference 7 and models $Df11_{Q2}$ and $Q2_{Df11}$ to model 2.2. No adjustments have been made to these models to correct for rated-speed open-circuit or on-line conditions.

ACKNOWLEDGMENTS

The author would like to thank the operations and commissioning staff at Atikokan for their assistance in the planning and execution of the standstill frequency response test.

Approved:

A. F. Baljet
Manager
Electrical Research Department

Submitted:

J. R. R. Service
Engineer - System Performance
System Studies Section

JRRS/jrrs

REFERENCES

1. Test Procedures for Synchronous Machines, IEEE Standard No 115-1983.

2. IEEE Standard Procedures for Obtaining Synchronous Machine Parameters by Standstill Frequency Response Testing (Supplement to ANSI/IEE Std 115-1983), IEEE Standard 115A-1987.

3. Coultes, M.E. et al, Determination of Synchronous Machine Stability Study Constants, Volume 2, EPRI EL-1424, December 1980.

4. Hooke, R., Jeeves T., Direct Search Solution of Numerical and Statistical Problems, J. Assoc. Comput., March 8, No 2, April 1961.

5. Rankin, A.W., Per-Unit Impedances of Synchronous Machines, AIEE Trans Vol 69, August 1945.

6. Rankin, A.W., Per-Unit Impedances of Synchronous Machines - II, AIEE Trans Vol 64, December 1945.

7. IEEE Committee Report, Current Usage and Suggested Practices in Power System Stability Simulations for Synchronous Machines, IEEE Trans, Vol EC-1, No 1, March 1986.

8. Minnich, S.H., Small Signals, Large Signals and Saturation in Generator Modelling, IEEE Trans, Vol EC-1, No 1, March 1986.

9. Canay, I.M., Identification and Determination of Synchronous Machine Parameters, Brown Boveri Review, June/July 1984.

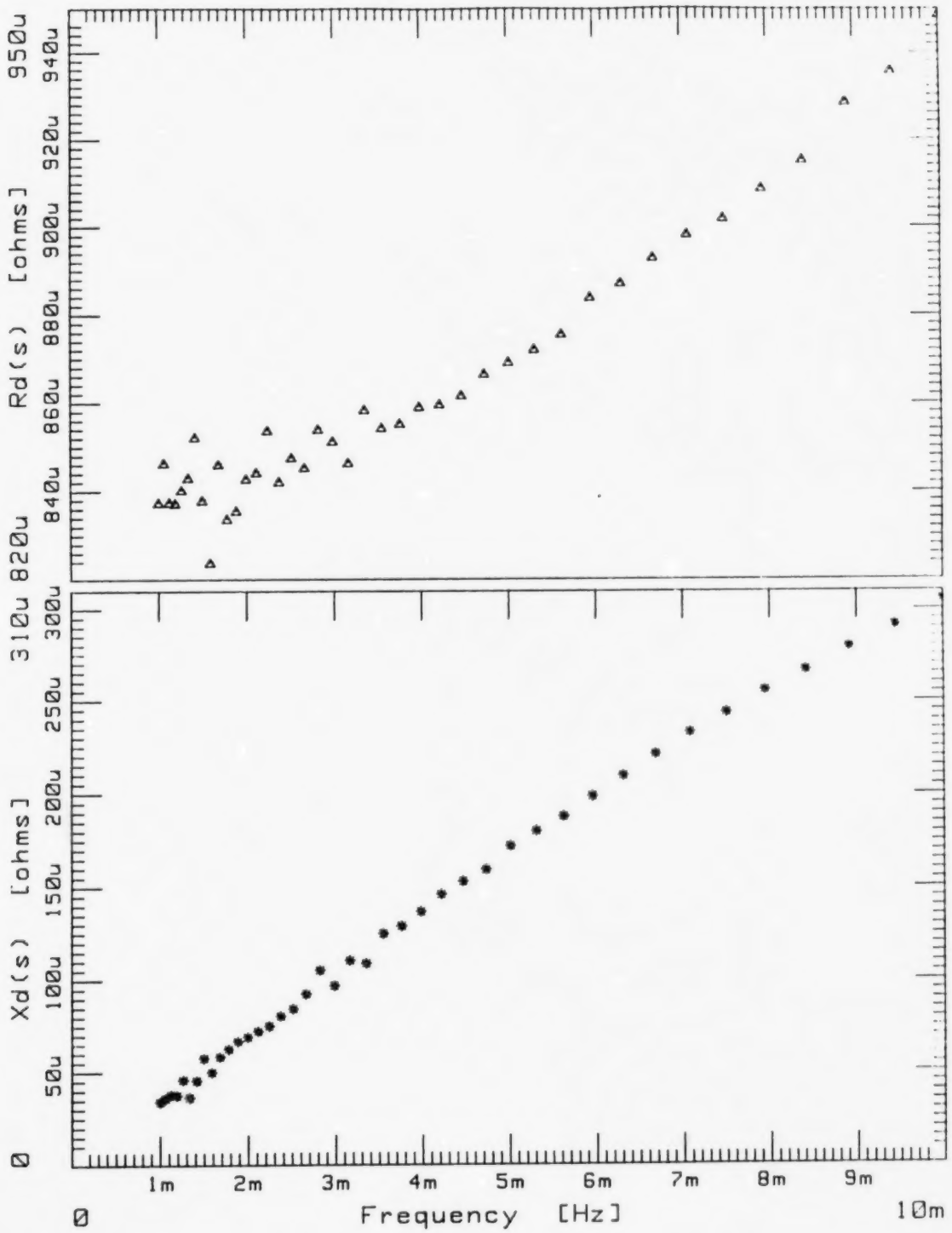

Figure 9: Low Frequency Direct Axis, Field Shorted, Impedance, $Z_d(s) = R_d(s) + jX_d(s)$ Resistance, $R_d(s)$ and Reactance, $X_d(s)$ vs. Frequency

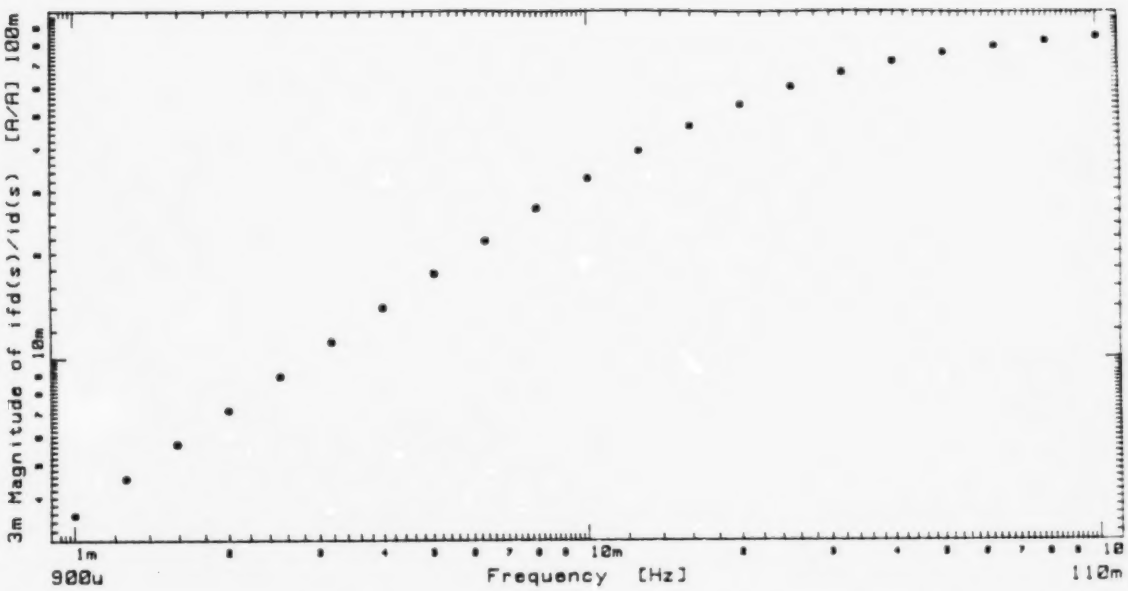

Figure 10: Field Current to Direct Axis Stator Current Transfer Function, $\Delta I_{fd}(s)/\Delta I_{d}(s)$ Magnitude vs. Low Frequency

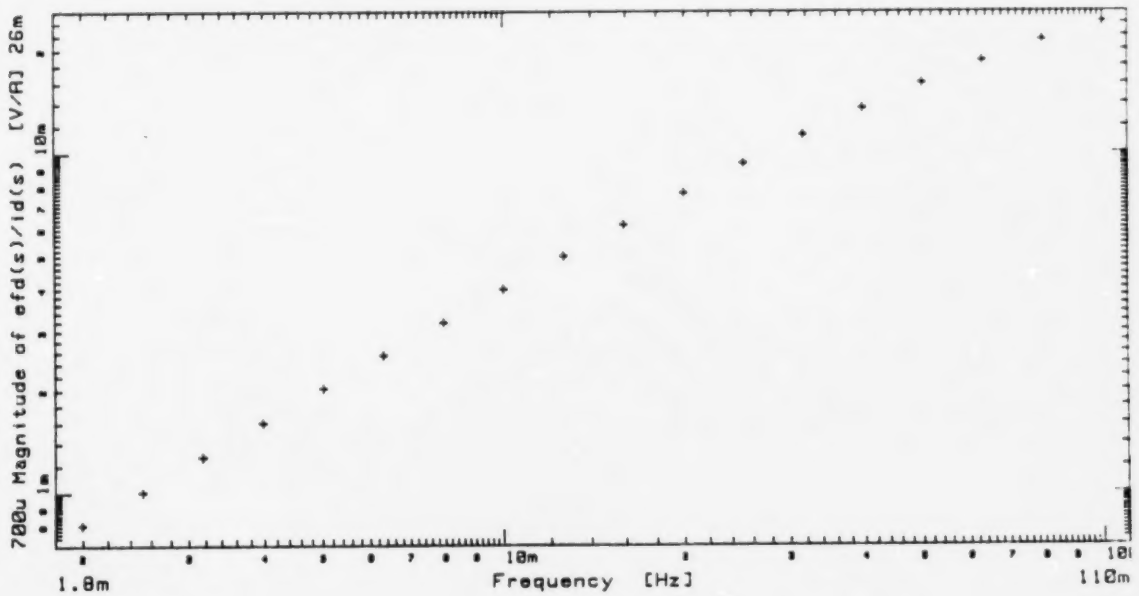

Figure 11: Field Voltage to Direct Axis Stator Current Transfer Function, $\Delta E_{fd}(s)/\Delta I_{d}(s)$ Magnitude vs. Low Frequency

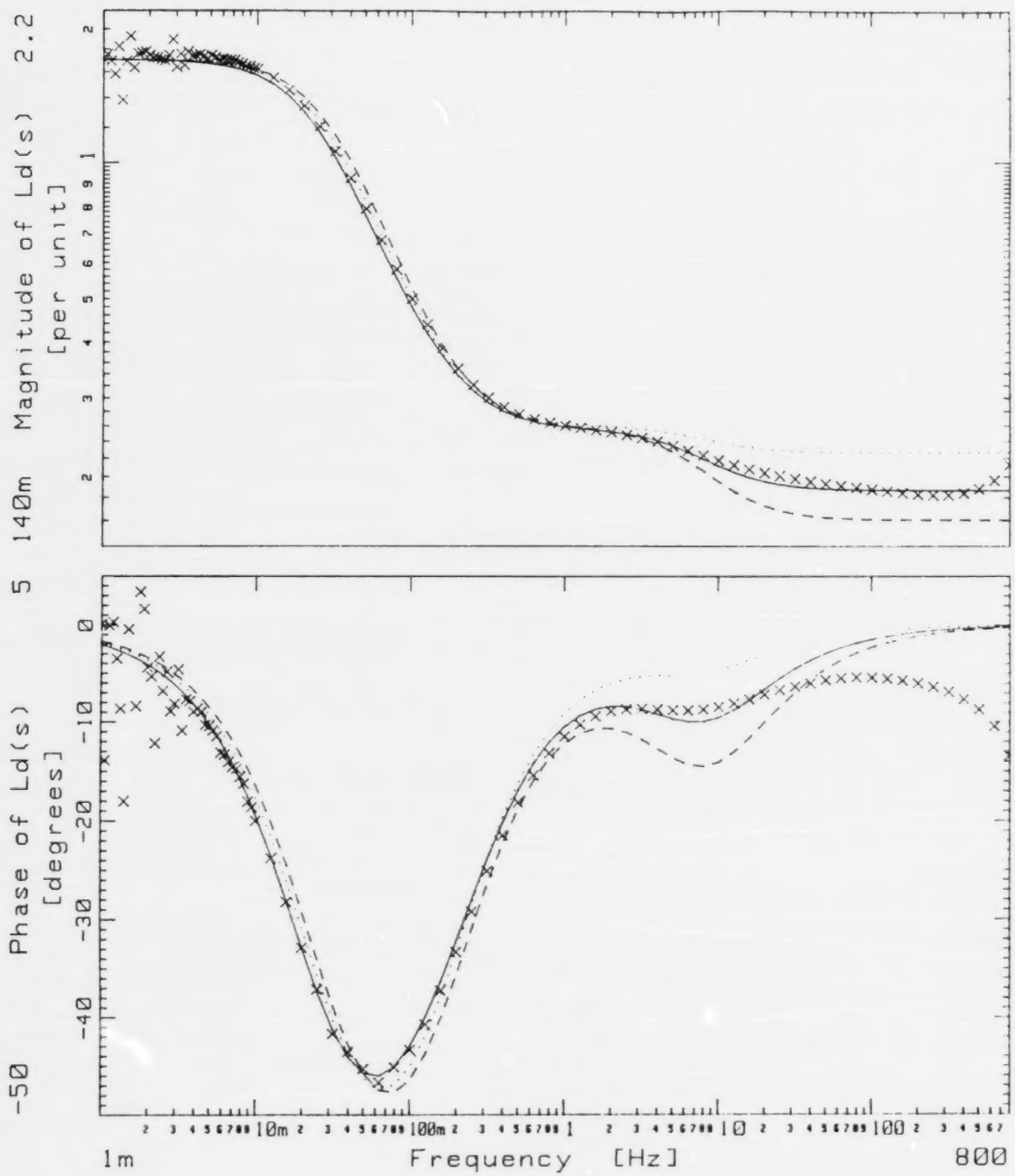

Figure 12: Comparison of SSFR Data with the Equivalent Circuit Models Responses for the Direct Axis, Field Shorted, Operational Inductance Under Standstill Test Conditions
LEGEND: SSFR Data xxxx ; Model $Df21_{Q3}$ ——— ; $Df11_{Q2}$ ····· ; $Df10_{Q2}$ - - - - -

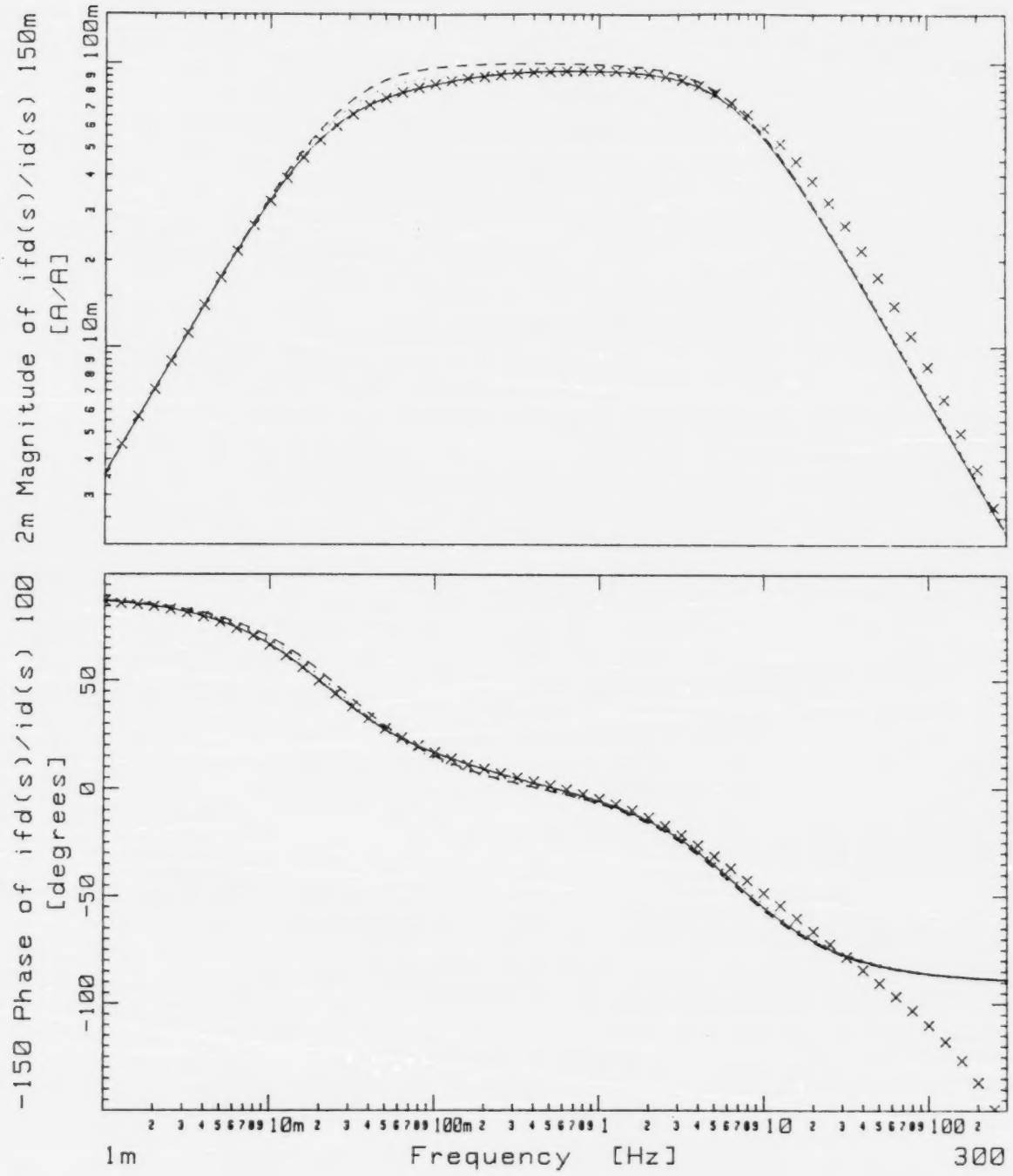

Figure 13: Comparison of SSFR Data with the Equivalent Circuit Models Responses for the Field Current to Direct Axis Stator Current Transfer Function Under Standstill Test Conditions

LEGEND: SSFR Data xxxx ; Model $Df21_{Q3}$ ——— ; $Df11_{Q2}$ ····· ; $Df10_{Q2}$ -----

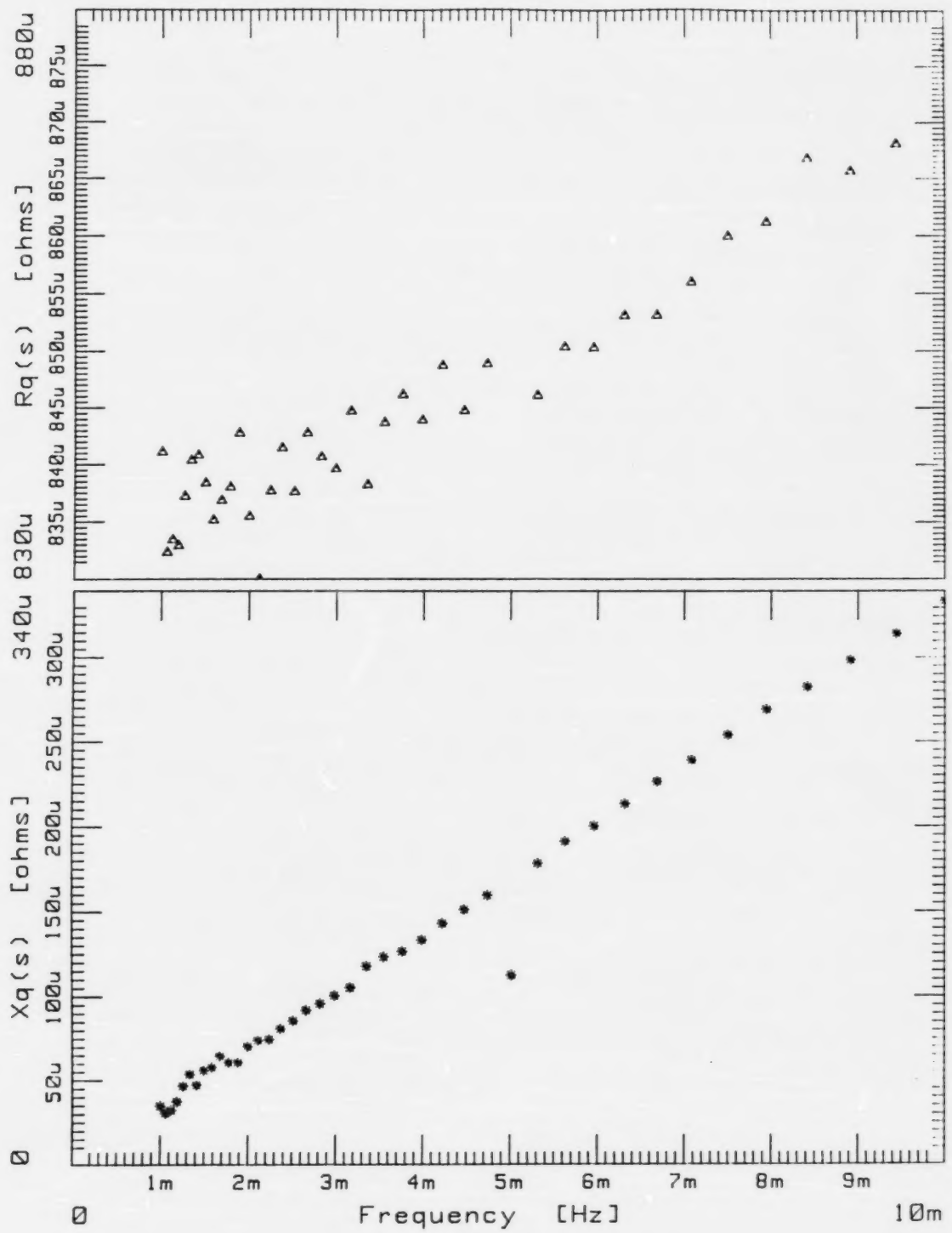

Figure 14: Low Frequency Quadrature Axis Impedance, $Z_q(s)$ Resistance, $R_q(s)$ and Reactance, $X_q(s)$ vs. Frequency

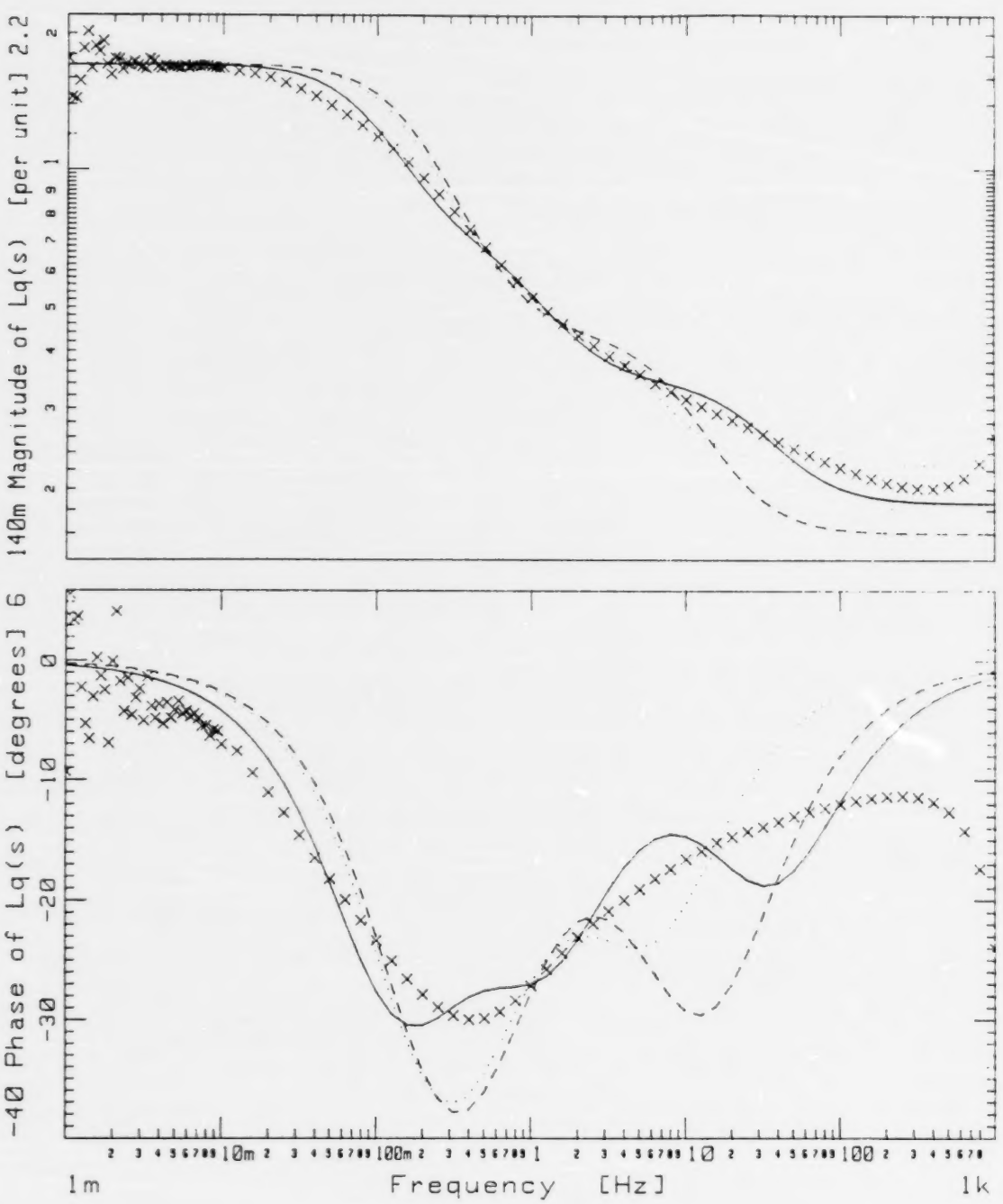

Figure 15: Comparison of SSFR Data with the Equivalent Circuit Models Responses for the Quadrature Axis Operational Inductance Under Standstill Test Conditions
LEGEND: SSFR Data xxxx ; Model $Q3_{Df21}$ ——— ; $Q2_{Df11}$ ····· ; $Q2_{Df10}$ -----

Appendix A: STANDSTILL FREQUENCY RESPONSE TEST DATA ATIKOKAN TGS

Table A-1: Direct Axis, Field Shorted, Test Data

Frequency Hz	Impedance Ohms	Phase Degrees	Inductance Per Unit	Phase Degrees	Ifd/Id A/A	Phase Degrees
0.001	8.382E-04	2.3	1.710	0.1	3.546E-03	87.5
0.001059	8.473E-04	2.4	1.754	-13.9		
0.001122	8.385E-04	2.6	1.693	-0.1		
0.001189	8.383E-04	2.6	1.583	0.3		
0.001259	8.417E-04	3.1	1.828	-3.5	4.522E-03	86.4
0.001334	8.440E-04	2.5	1.386	-8.7		
0.001413	8.536E-04	3.1	1.693	-18.0		
0.001496	8.401E-04	3.9	1.927	-0.5		
0.001585	8.255E-04	3.5	1.637	15.3	5.680E-03	85.7
0.001679	8.483E-04	4.0	1.761	-8.4		
0.001778	8.363E-04	4.3	1.768	3.4		
0.001884	8.384E-04	4.6	1.780	1.6		
0.001995	8.458E-04	4.7	1.745	-4.4	7.090E-03	84.8
0.002113	8.475E-04	4.9	1.724	-5.4		
0.002239	8.572E-04	5.0	1.723	-12.2		
0.002371	8.462E-04	5.5	1.705	-3.3		
0.002512	8.520E-04	5.7	1.697	-6.8	8.886E-03	83.5
0.002661	8.506E-04	6.3	1.747	-4.9		
0.002818	8.607E-04	7.0	1.895	-8.9		
0.002985	8.570E-04	6.5	1.642	-8.2		
0.003162	8.538E-04	7.5	1.757	-4.6	1.115E-02	81.8
0.00335	8.655E-04	7.2	1.657	-10.9		
0.003548	8.636E-04	8.3	1.780	-7.7		
0.003758	8.651E-04	8.6	1.735	-7.9		
0.003981	8.701E-04	9.1	1.742	-9.0	1.397E-02	80.0
0.004217	8.721E-04	9.6	1.753	-8.6		
0.004467	8.753E-04	10.1	1.735	-9.0		
0.004732	8.812E-04	10.4	1.712	-10.3		
0.005012	8.862E-04	11.2	1.744	-10.4	1.742E-02	77.5
0.005309	8.906E-04	11.7	1.727	-10.9		
0.005623	8.956E-04	12.1	1.704	-11.5		
0.005957	9.060E-04	12.7	1.711	-13.2		
0.00631	9.116E-04	13.3	1.705	-13.3	2.157E-02	74.4
0.006683	9.199E-04	13.9	1.704	-14.1		
0.007079	9.280E-04	14.5	1.699	-14.6		
0.007499	9.343E-04	15.1	1.679	-14.8		
0.007943	9.440E-04	15.7	1.669	-15.6	2.664E-02	70.9
0.008414	9.533E-04	16.2	1.649	-16.3		
0.008913	9.697E-04	16.7	1.647	-18.1		
0.009441	9.800E-04	17.3	1.627	-18.6		
0.01	9.967E-04	17.8	1.625	-20.0	3.248E-02	66.6
0.01259	1.058E-03	19.8	1.554	-23.8	3.906E-02	61.6
0.01585	1.132E-03	21.1	1.458	-28.2	4.611E-02	56.0
0.01995	1.215E-03	21.8	1.343	-32.9	5.329E-02	50.0
0.02512	1.297E-03	21.9	1.207	-37.1	6.002E-02	43.9
0.03162	1.377E-03	21.3	1.060	-41.7	6.606E-02	38.0
0.03981	1.447E-03	21.6	0.925	-43.6	7.120E-02	32.5
0.05012	1.510E-03	21.7	0.793	-45.3	7.555E-02	27.7

Direct Axis, Field Shorted, Test Data

Frequency Hz	Impedance Ohms	Phase Degrees	Inductance Per Unit	Phase Degrees	Ifd/Id A/A	Phase Degrees
0.0631	1.570E-03	21.8	0.675	-46.7	7.909E-02	23.4
0.07943	1.628E-03	23.6	0.581	-45.1	8.204E-02	19.7
0.1	1.688E-03	25.5	0.500	-43.3	8.443E-02	16.4
0.1259	1.766E-03	28.2	0.438	-40.7	8.669E-02	13.6
0.1585	1.859E-03	31.7	0.388	-37.3	8.857E-02	10.8
0.1995	1.979E-03	36.0	0.349	-33.3	8.980E-02	8.9
0.2512	2.150E-03	40.9	0.321	-29.2	9.110E-02	6.9
0.3162	2.379E-03	46.3	0.300	-25.1	9.209E-02	5.0
0.3981	2.702E-03	51.7	0.286	-21.5	9.296E-02	3.2
0.5012	3.132E-03	57.1	0.276	-18.2	9.365E-02	1.4
0.631	3.707E-03	62.0	0.269	-15.5	9.410E-02	-0.5
0.7943	4.461E-03	66.2	0.264	-13.2	9.433E-02	-2.5
1	5.432E-03	69.8	0.260	-11.5	9.439E-02	-4.8
1.259	6.675E-03	72.6	0.257	-10.3	9.412E-02	-7.3
1.585	8.240E-03	74.8	0.254	-9.5	9.339E-02	-10.2
1.995	1.019E-02	76.4	0.251	-8.9	9.200E-02	-13.5
2.512	1.261E-02	77.5	0.248	-8.7	8.997E-02	-17.3
3.162	1.558E-02	78.3	0.244	-8.7	8.708E-02	-21.6
3.981	1.921E-02	78.8	0.239	-8.8	8.315E-02	-26.4
5.012	2.360E-02	79.1	0.234	-8.9	7.814E-02	-31.5
6.31	2.898E-02	79.5	0.229	-8.9	7.244E-02	-37.0
7.943	3.556E-02	79.9	0.223	-8.8	6.592E-02	-42.7
10	4.362E-02	80.4	0.217	-8.5	5.898E-02	-48.5
12.59	5.359E-02	81.0	0.212	-8.1	5.190E-02	-54.4
15.85	6.600E-02	81.6	0.208	-7.7	4.495E-02	-60.4
19.95	8.151E-02	82.2	0.204	-7.2	3.836E-02	-66.4
25.12	1.010E-01	82.8	0.201	-6.8	3.218E-02	-72.3
31.62	1.253E-01	83.2	0.198	-6.4	2.662E-02	-78.3
39.81	1.554E-01	83.6	0.195	-6.1	2.170E-02	-84.3
50.12	1.934E-01	84.0	0.193	-5.7	1.747E-02	-90.4
63.1	2.411E-01	84.3	0.191	-5.5	1.389E-02	-96.6
79.43	3.005E-01	84.4	0.189	-5.5	1.094E-02	-103.1
100	3.746E-01	84.4	0.187	-5.5	8.511E-03	-110.1
125.9	4.672E-01	84.3	0.186	-5.6	6.554E-03	-117.7
158.5	5.832E-01	84.2	0.184	-5.8	4.973E-03	-126.6
199.5	7.291E-01	83.9	0.183	-6.0	3.717E-03	-136.9
251.2	9.144E-01	83.5	0.182	-6.4	2.729E-03	-149.5
316.2	1.152E+00	83.0	0.182	-6.9	1.937E-03	-164.1
398.1	1.463E+00	82.3	0.184	-7.6	1.361E-03	179.2
501.2	1.883E+00	81.2	0.188	-8.7	9.719E-04	164.0
631	2.477E+00	79.5	0.196	-10.5	7.419E-04	150.3
794.3	3.377E+00	76.5	0.213	-13.5	6.960E-04	147.7

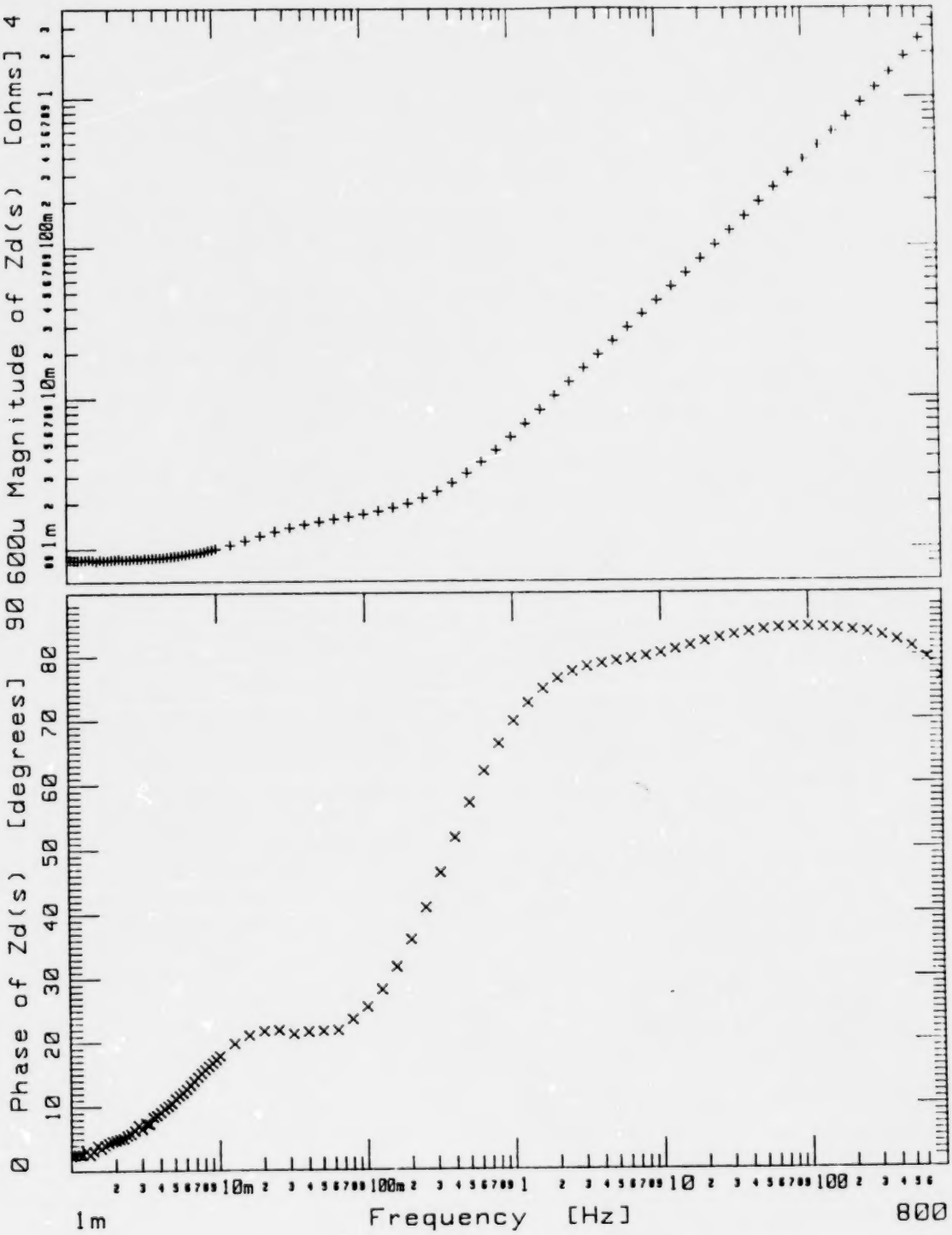

Figure A-1: Direct Axis Impedance, Field Shorted, $Z_d(s)$ Magnitude and Phase vs. Frequency

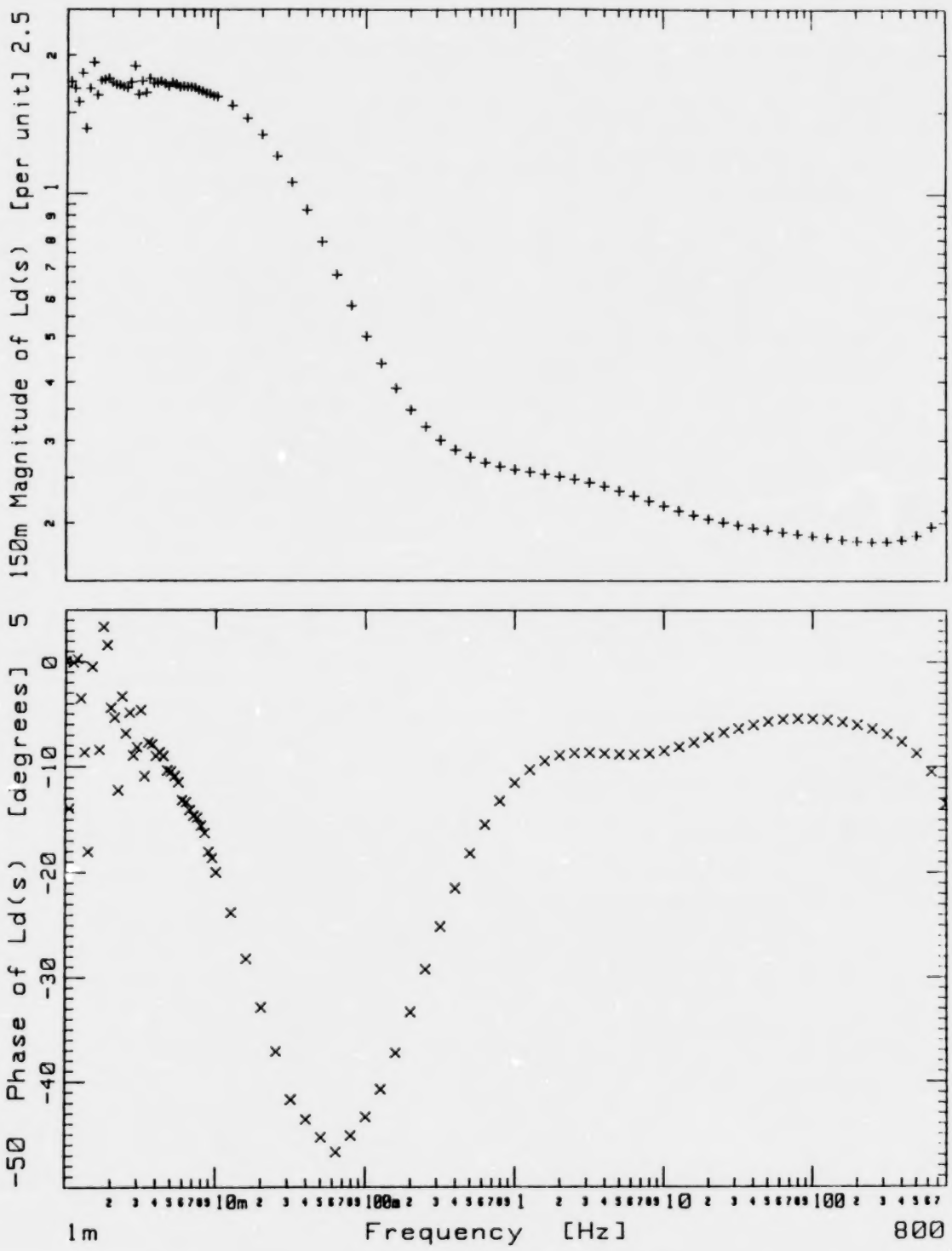

Figure A-2: Direct Axis Operational Inductance, Field Shorted, $L_d(s)$ Magnitude and Phase vs. Frequency

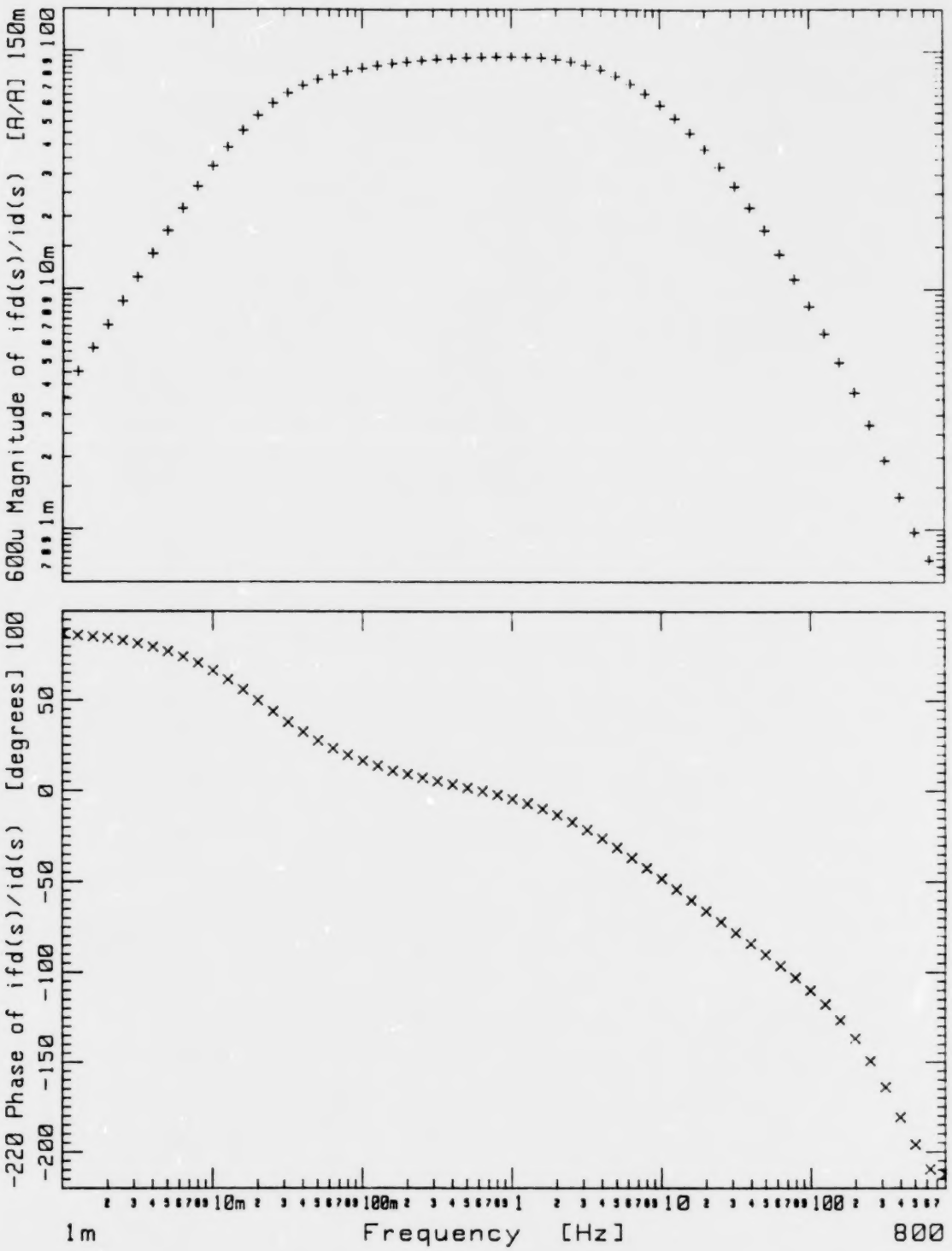

Figure A-3: Field Current to Direct Axis Stator Current Transfer Function, $\Delta I_{fd}(s)/\Delta I_{d}(s)$ Magnitude and Phase vs. Frequency

Table A-2: Direct Axis, Field Open, Test Data

Frequency Hz	Impedance Ohms	Phase Degrees	Inductance Per Unit	Phase Degrees	Ifd/Id A/A	Phase Degrees
0.001585	8.515E-04	3.6	1.717	-13.0	3.546E-03	87.5
0.001995	8.393E-04	4.8	1.765	1.0	8.050E-04	87.4
0.002512	8.391E-04	6.0	1.755	2.0	1.006E-03	87.6
0.003162	8.496E-04	7.6	1.788	-2.3	1.277E-03	87.0
0.003981	8.522E-04	9.4	1.745	-1.3	1.604E-03	86.4
0.005012	8.686E-04	11.7	1.757	-4.2	2.025E-03	85.6
0.00631	8.837E-04	14.3	1.738	-4.9	2.541E-03	84.5
0.007943	9.067E-04	17.8	1.753	-5.3	3.177E-03	83.3
0.01	9.454E-04	21.6	1.754	-6.8	3.980E-03	81.7
0.01259	1.003E-03	25.5	1.737	-8.9	4.966E-03	80.0
0.01585	1.077E-03	29.6	1.705	-10.6	6.151E-03	77.5
0.01995	1.185E-03	33.2	1.672	-13.3	7.606E-03	74.7
0.02512	1.321E-03	36.6	1.629	-15.8	9.306E-03	71.6
0.03162	1.490E-03	39.2	1.571	-18.6	1.127E-02	68.0
0.03981	1.698E-03	40.9	1.504	-21.9	1.349E-02	64.1
0.05012	1.931E-03	41.8	1.418	-25.0	1.594E-02	60.1
0.0631	2.187E-03	42.1	1.318	-28.1	1.853E-02	55.9
0.07943	2.469E-03	42.0	1.214	-31.2	2.131E-02	51.7
0.1	2.774E-03	41.5	1.108	-34.0	2.420E-02	47.6
0.1259	3.090E-03	40.9	1.000	-36.5	2.713E-02	43.4
0.1585	3.421E-03	40.3	0.894	-38.7	3.008E-02	39.4
0.1995	3.760E-03	39.9	0.793	-40.4	3.292E-02	35.4
0.2512	4.112E-03	39.7	0.698	-41.5	3.565E-02	31.7
0.3162	4.480E-03	40.0	0.613	-42.0	3.820E-02	28.1
0.3981	4.873E-03	40.8	0.537	-41.8	4.052E-02	24.7
0.5012	5.307E-03	42.3	0.471	-40.9	4.264E-02	21.6
0.631	5.807E-03	44.4	0.415	-39.2	4.453E-02	18.7
0.7943	6.408E-03	47.1	0.370	-36.9	4.616E-02	16.0
1	7.158E-03	50.4	0.333	-34.0	4.762E-02	13.5
1.259	8.110E-03	54.0	0.304	-30.9	4.887E-02	11.2
1.585	9.335E-03	57.8	0.281	-27.7	4.997E-02	9.0
1.995	1.090E-02	61.5	0.264	-24.5	5.081E-02	6.9
2.512	1.292E-02	65.0	0.251	-21.6	5.159E-02	4.8
3.162	1.548E-02	68.2	0.240	-18.9	5.214E-02	2.7
3.981	1.873E-02	71.0	0.232	-16.6	5.245E-02	0.5
5.012	2.280E-02	73.4	0.225	-14.6	5.249E-02	-1.7
6.31	2.789E-02	75.4	0.219	-12.9	5.223E-02	-4.0
7.943	3.430E-02	77.2	0.215	-11.4	5.181E-02	-6.4
10	4.234E-02	78.7	0.211	-10.2	5.120E-02	-9.0
12.59	5.230E-02	80.0	0.207	-9.1	5.022E-02	-11.6
15.85	6.482E-02	81.1	0.204	-8.2	4.913E-02	-14.4
19.95	8.041E-02	82.0	0.201	-7.4	4.784E-02	-17.6
25.12	1.001E-01	82.7	0.199	-6.8	4.635E-02	-21.2
31.62	1.246E-01	83.3	0.197	-6.3	4.458E-02	-25.3
39.81	1.547E-01	83.8	0.194	-5.9	4.237E-02	-29.8
50.12	1.930E-01	84.1	0.192	-5.6	3.988E-02	-35.0
63.1	2.406E-01	84.4	0.191	-5.4	3.718E-02	-41.2
79.43	2.644E-01	82.8	0.189	-5.4	3.399E-02	-48.1

Direct Axis, Field Open, Test Data

Frequency Hz	Impedance Ohms	Phase Degrees	Inductance Per Unit	Phase Degrees	Ifd/Id A/A	Phase Degrees
100	3.744E-01	84.4	0.187	-5.4	3.079E-02	-55.1
125.9	4.670E-01	84.4	0.185	-5.5	2.735E-02	-63.1
158.5	5.831E-01	84.2	0.184	-5.7	2.386E-02	-72.2
199.5	7.286E-01	83.9	0.183	-6.0	2.039E-02	-82.4
251.2	9.137E-01	83.6	0.182	-6.4	1.694E-02	-94.3
316.2	1.151E+00	83.1	0.182	-6.9	1.354E-02	-107.8
398.1	1.461E+00	82.4	0.183	-7.6	1.025E-02	-123.4
501.2	1.878E+00	81.4	0.187	-8.6	7.175E-03	-141.1
631	2.468E+00	79.7	0.196	-10.2	4.441E-03	-161.7
794.3	3.357E+00	76.8	0.211	-13.2	2.194E-03	171.9
1000	4.774E+00	71.4	0.239	-18.6	5.762E-04	103.4

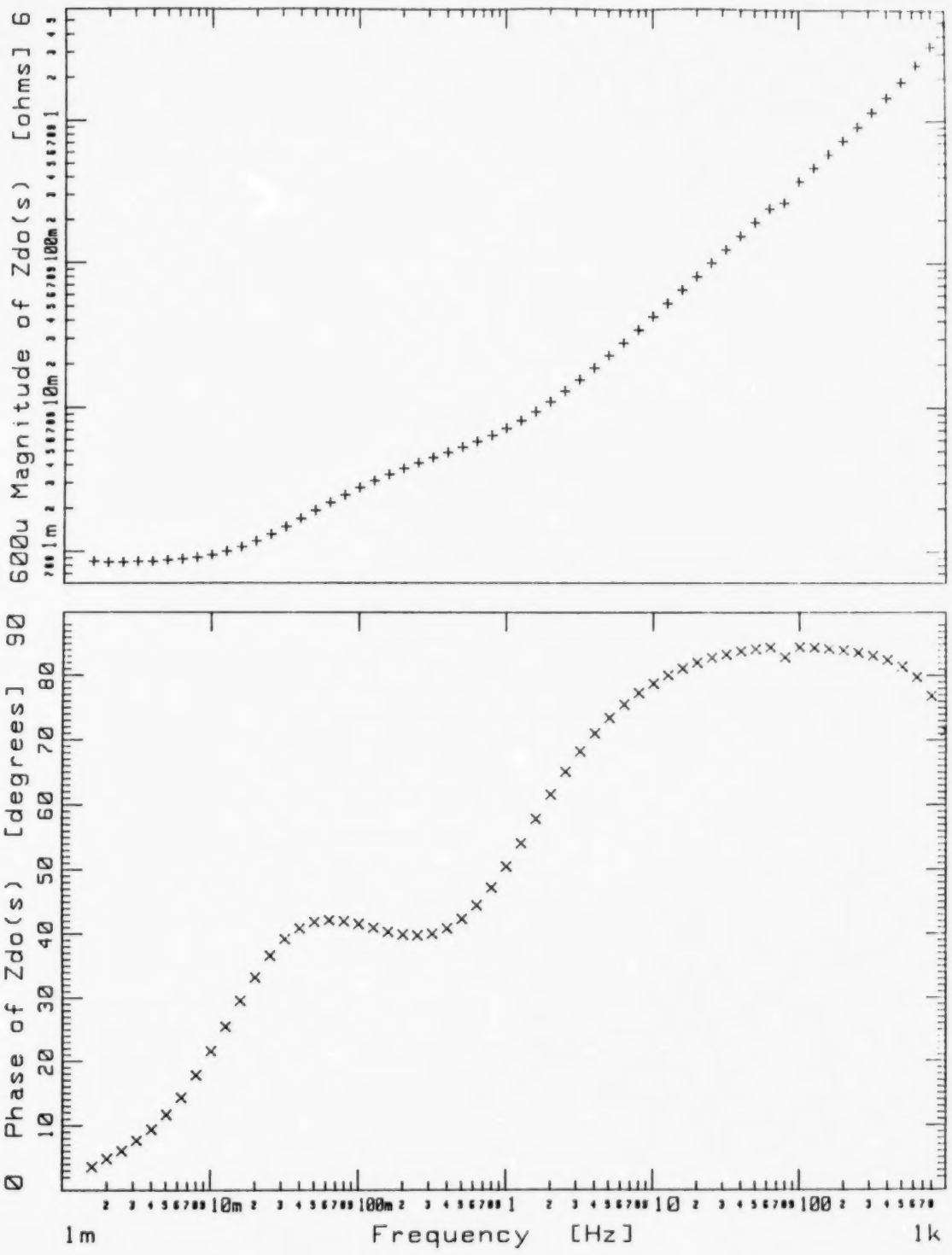

Figure A-4: Direct Axis Impedance, Field Open, $Z_{do}(s)$ Magnitude and Phase vs. Frequency

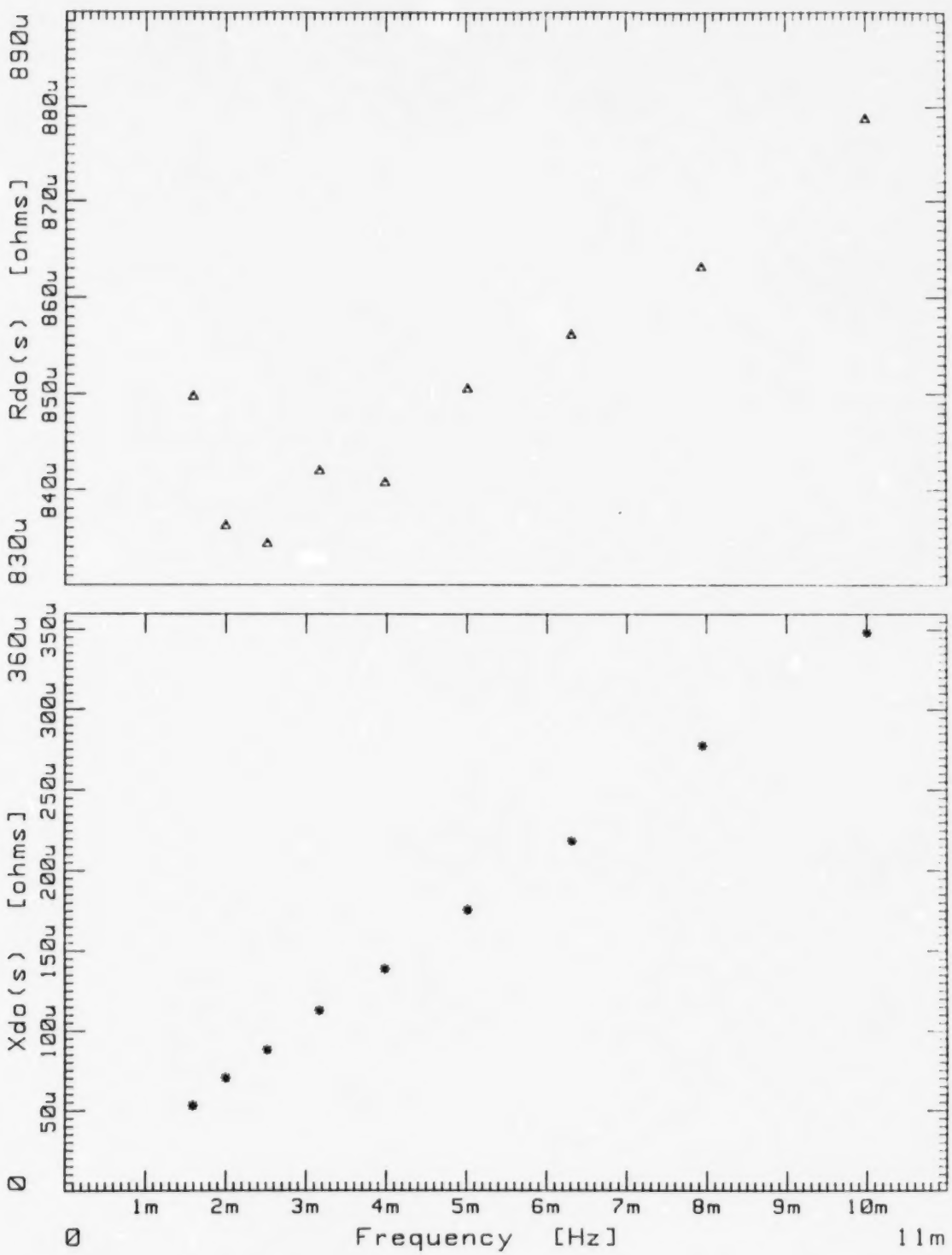

Figure A-5: Low Frequency Direct Axis, Field Open, Impedance Resistance, $R_{do}(s)$ and Reactance, $X_{do}(s)$ vs. Frequency

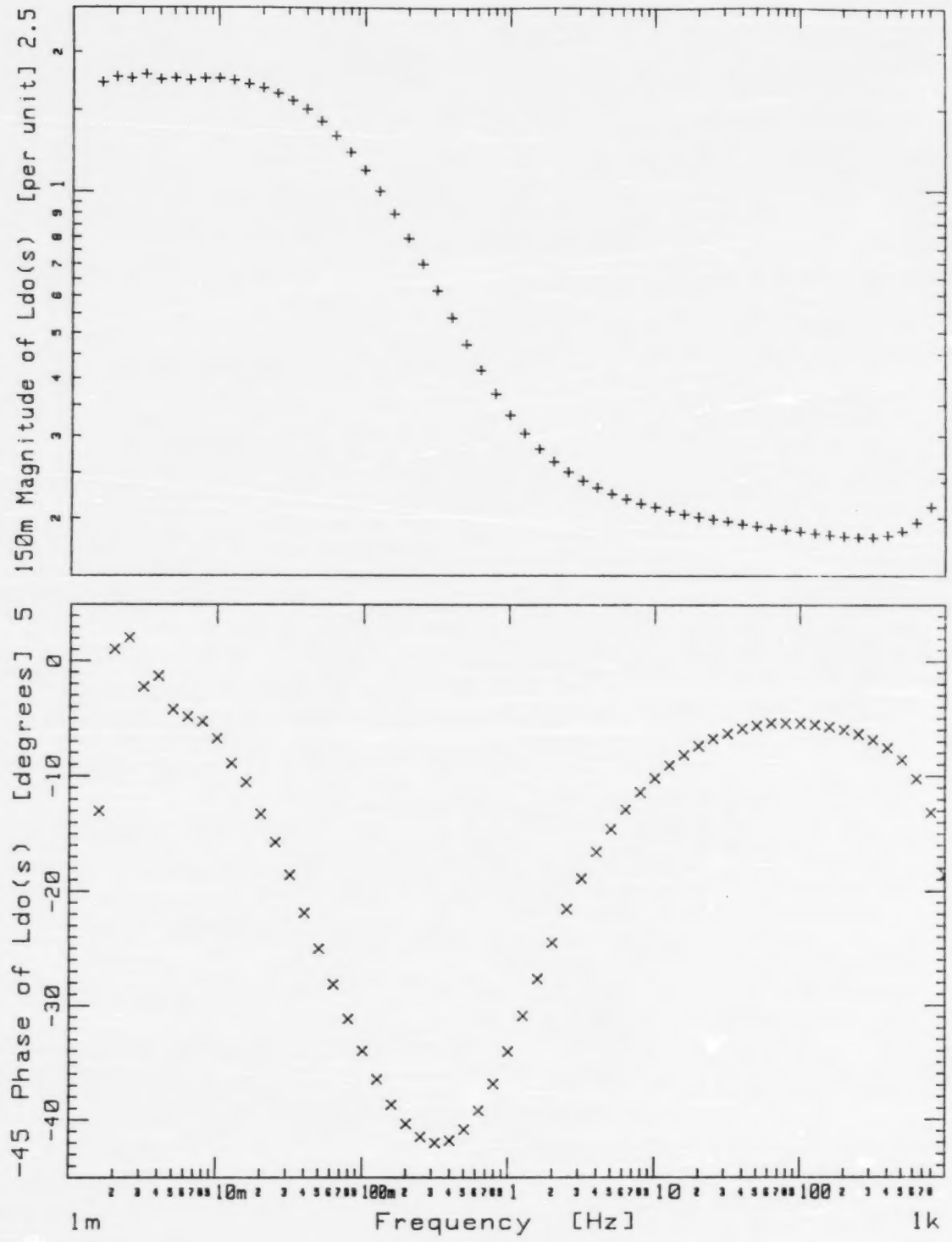

Figure A-6: Direct Axis Operational Inductance, Field Open, $L_{do}(s)$ Magnitude and Phase vs. Frequency

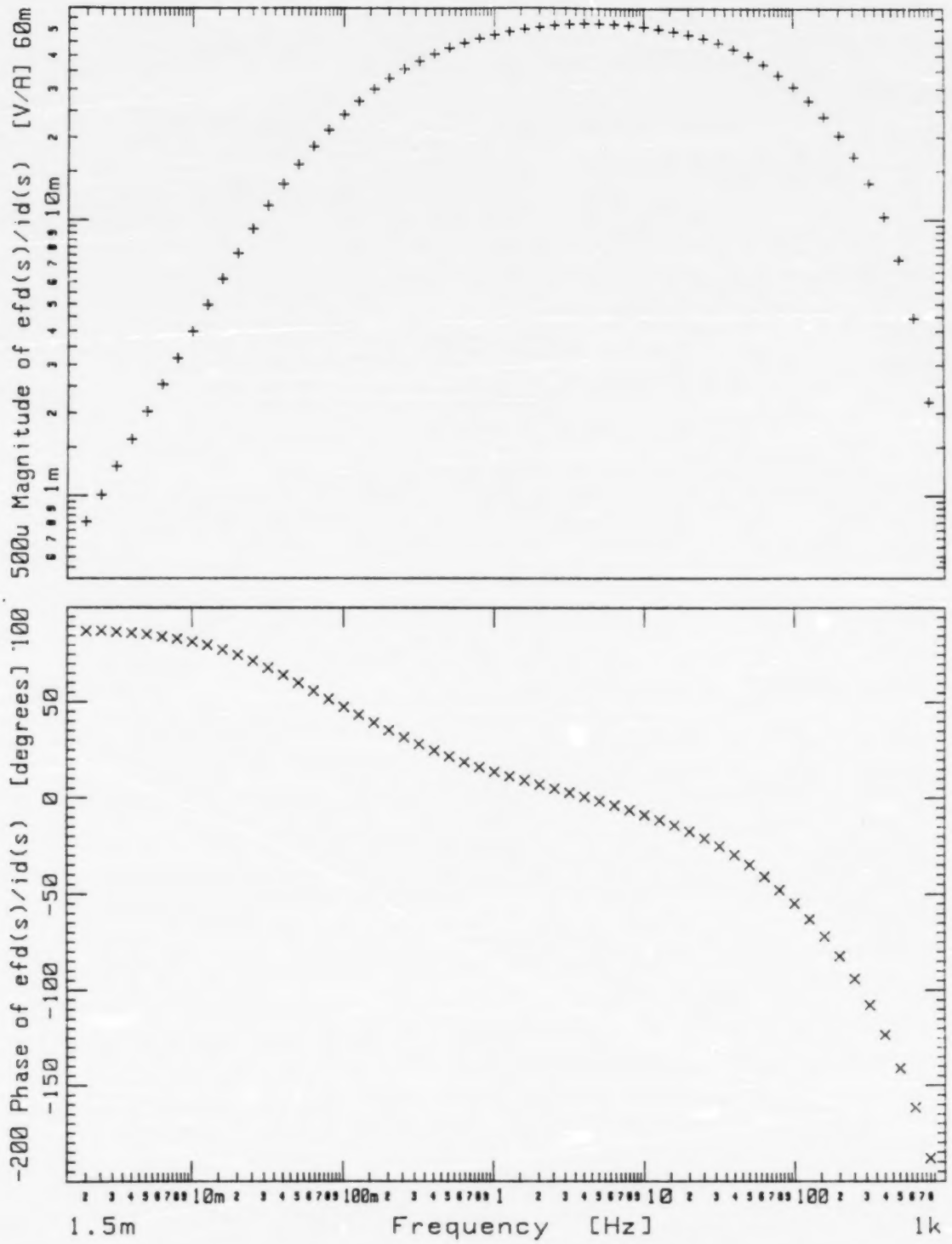

Figure A-7: Field Voltage to Direct Axis Stator Current Transfer Function, $\Delta E_{fd}(s)/\Delta I_d(s)$ Magnitude and Phase vs. Frequency

Table A-3: Quadrature Axis, Test Data

Frequency Hz	Impedance Ohms	Phase Degrees	Inductance Per Unit	Phase Degrees
0.001	8.419E-04	2.4	1.765	-9.3
0.001059	8.330E-04	2.1	1.453	5.7
0.001122	8.342E-04	2.2	1.441	3.4
0.001189	8.339E-04	2.6	1.577	3.8
0.001259	8.386E-04	3.2	1.855	-2.3
0.001334	8.422E-04	3.7	2.019	-5.3
0.001413	8.423E-04	3.2	1.681	-6.6
0.001496	8.404E-04	3.8	1.877	-3.1
0.001585	8.373E-04	4.0	1.826	0.2
0.001679	8.395E-04	4.4	1.924	-1.3
0.001778	8.403E-04	4.1	1.711	-2.5
0.001884	8.451E-04	4.1	1.625	-6.9
0.001995	8.386E-04	4.8	1.764	-0.1
0.002113	8.334E-04	5.1	1.757	4.2
0.002239	8.411E-04	5.1	1.669	-1.8
0.002371	8.455E-04	5.5	1.715	-4.3
0.002512	8.421E-04	5.8	1.708	-1.5
0.002661	8.479E-04	6.2	1.736	-4.6
0.002818	8.462E-04	6.5	1.705	-3.2
0.002985	8.457E-04	6.8	1.687	-2.4
0.003162	8.514E-04	7.1	1.672	-5.1
0.00335	8.466E-04	8.0	1.760	-1.4
0.003548	8.528E-04	8.3	1.742	-3.9
0.003758	8.557E-04	8.5	1.688	-4.9
0.003981	8.545E-04	9.0	1.676	-3.7
0.004217	8.608E-04	9.6	1.702	-5.3
0.004467	8.583E-04	10.1	1.694	-3.5
0.004732	8.638E-04	10.6	1.691	-4.8
0.005012	7.856E-04	8.2	1.687	-4.2
0.005309	8.647E-04	11.9	1.680	-3.4
0.005623	8.716E-04	12.7	1.703	-4.5
0.005957	8.736E-04	13.2	1.684	-4.3
0.00631	8.794E-04	14.0	1.695	-4.7
0.006683	8.827E-04	14.8	1.697	-4.5
0.007079	8.887E-04	15.6	1.692	-4.9
0.007499	8.967E-04	16.4	1.699	-5.5
0.007943	9.023E-04	17.3	1.700	-5.5
0.008414	9.117E-04	18.0	1.688	-6.3
0.008913	9.157E-04	19.0	1.682	-5.8
0.009441	9.234E-04	19.9	1.674	-5.9
0.01	9.383E-04	20.9	1.683	-7.1
0.01259	9.815E-04	24.9	1.653	-7.6
0.01585	1.052E-03	29.0	1.631	-9.5
0.01995	1.146E-03	33.2	1.604	-11.1
0.02512	1.266E-03	37.2	1.561	-12.8
0.03162	1.420E-03	40.7	1.512	-14.6
0.03981	1.611E-03	43.7	1.458	-16.5

Quadrature Axis Test Data

Frequency Hz	Impedance Ohms	Phase Degrees	Inductance Per Unit	Phase Degrees
0.05012	1.837E-03	46.2	1.392	-18.2
0.0631	2.110E-03	48.2	1.326	-20.0
0.07943	2.431E-03	49.7	1.256	-21.7
0.1	2.805E-03	50.8	1.183	-23.4
0.1259	3.243E-03	51.5	1.112	-25.0
0.1585	3.738E-03	51.9	1.037	-26.6
0.1995	4.276E-03	52.2	0.958	-27.9
0.2512	4.897E-03	52.5	0.883	-28.9
0.3162	5.576E-03	52.9	0.809	-29.6
0.3981	6.338E-03	53.5	0.738	-30.0
0.5012	7.211E-03	54.3	0.674	-29.9
0.631	8.232E-03	55.6	0.617	-29.3
0.7943	9.445E-03	57.2	0.568	-28.4
1	1.090E-02	58.9	0.524	-27.2
1.259	1.269E-02	60.8	0.489	-25.8
1.585	1.494E-02	62.7	0.460	-24.4
1.995	1.760E-02	64.4	0.433	-23.1
2.512	2.099E-02	65.9	0.411	-22.0
3.162	2.498E-02	67.3	0.390	-20.9
3.981	2.990E-02	68.5	0.372	-20.0
5.012	3.595E-02	69.6	0.356	-19.1
6.31	4.314E-02	70.7	0.340	-18.2
7.943	5.214E-02	71.7	0.327	-17.4
10	6.304E-02	72.7	0.314	-16.6
12.59	7.659E-02	73.5	0.303	-15.9
15.85	9.291E-02	74.3	0.292	-15.2
19.95	1.132E-01	74.9	0.283	-14.7
25.12	1.376E-01	75.4	0.273	-14.3
31.62	1.670E-01	75.8	0.264	-13.9
39.81	2.026E-01	76.3	0.254	-13.5
50.12	2.462E-01	76.8	0.245	-13.0
63.1	2.998E-01	77.2	0.237	-12.7
79.43	3.653E-01	77.5	0.230	-12.3
100	4.457E-01	77.9	0.223	-12.0
125.9	5.453E-01	78.2	0.216	-11.8
158.5	6.690E-01	78.4	0.211	-11.5
199.5	8.238E-01	78.5	0.206	-11.4
251.2	1.020E+00	78.6	0.203	-11.4
316.2	1.270E+00	78.5	0.201	-11.5
398.1	1.598E+00	78.1	0.201	-11.9
501.2	2.041E+00	77.3	0.204	-12.7
631	2.668E+00	75.7	0.211	-14.3
794.3	3.620E+00	72.6	0.228	-17.4
1000	5.229E+00	66.0	0.261	-24.0

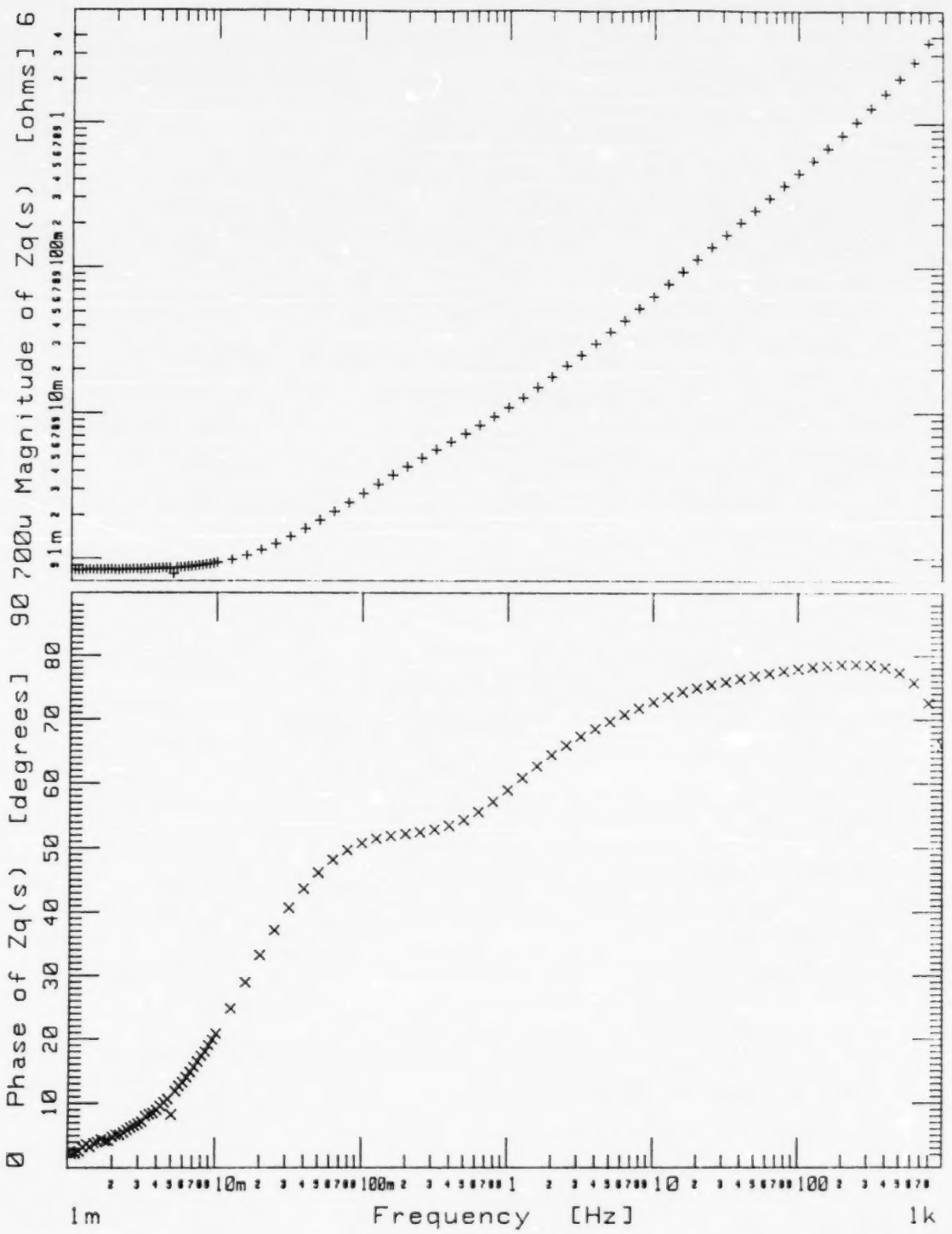

Figure A-8: Quadrature Axis Impedance, $Z_q(s)$, Magnitude and Phase vs. Frequency

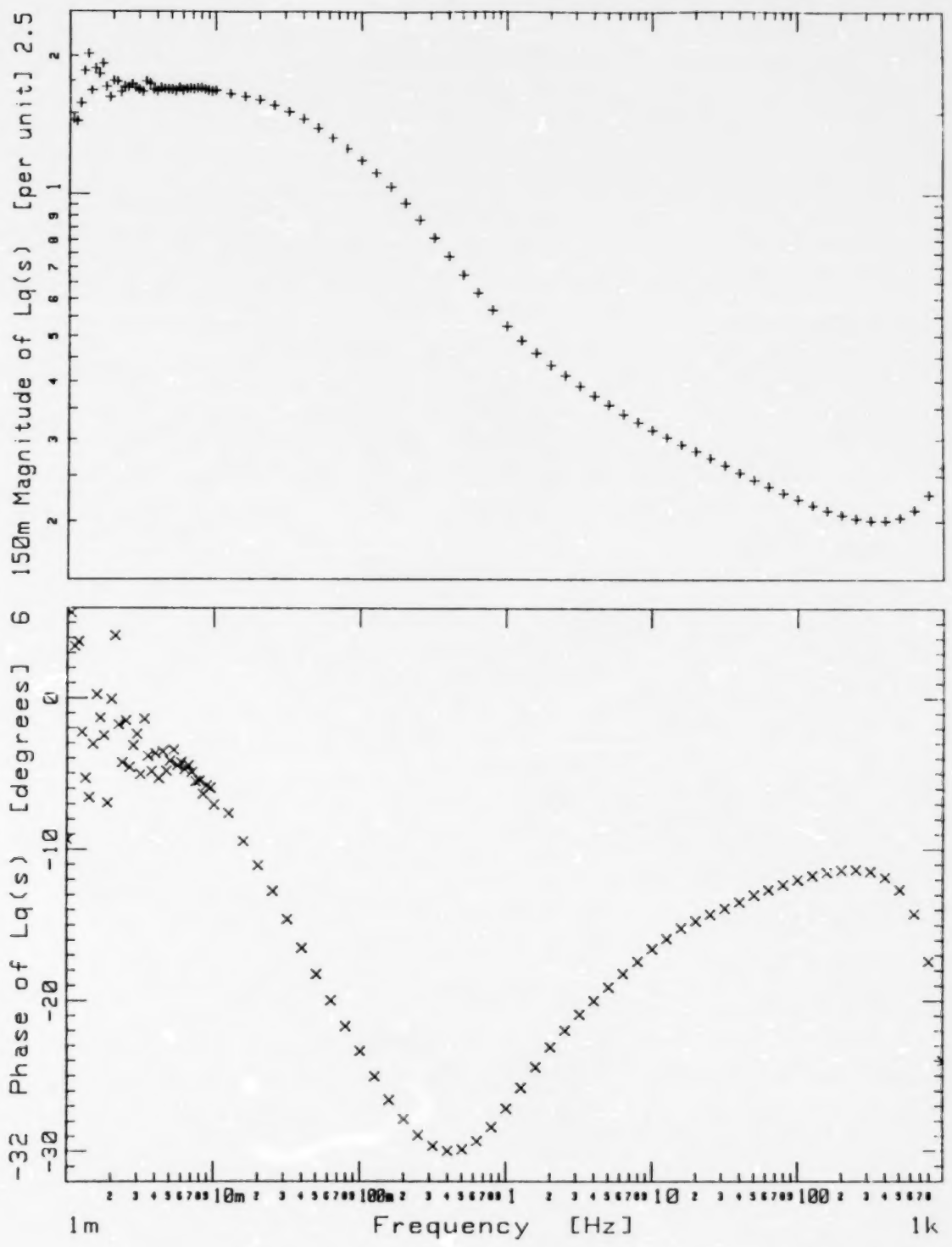

Figure A-9: Quadrature Axis Operational Inductance, $L_q(s)$ Magnitude and Phase vs. Frequency

Table A-4: Field Impedance, Stator Open, Test Data

Frequency Hz	Impedance Ohms	Phase Degrees
0.001	9.913E-02	2.3
0.001259	9.973E-02	2.8
0.001585	9.979E-02	3.6
0.001995	9.967E-02	4.5
0.002512	1.002E-01	5.5
0.003162	1.010E-01	6.9
0.003981	1.017E-01	8.6
0.005012	1.031E-01	10.7
0.00631	1.050E-01	13.3
0.007943	1.078E-01	16.2
0.01	1.121E-01	19.5
0.01259	1.186E-01	23.1
0.01585	1.266E-01	26.8
0.01995	1.374E-01	30.3
0.02512	1.527E-01	33.3
0.03162	1.714E-01	35.6
0.03981	1.930E-01	37.0
0.05012	2.189E-01	37.5
0.0631	2.467E-01	37.2
0.07943	2.768E-01	36.1
0.1	3.077E-01	34.5
0.1259	3.383E-01	32.6
0.1585	3.686E-01	30.4
0.1995	3.957E-01	28.2
0.2512	4.223E-01	26.0
0.3162	4.461E-01	24.1
0.3981	4.674E-01	22.3
0.5012	4.872E-01	20.9
0.631	5.054E-01	19.8
0.7943	5.216E-01	19.1
1	5.370E-01	18.9
1.259	5.535E-01	19.1
1.585	5.705E-01	19.8
1.995	5.897E-01	21.1
2.512	6.122E-01	22.9
3.162	6.402E-01	25.1
3.981	6.755E-01	27.8
5.012	7.206E-01	30.8
6.31	7.780E-01	34.0
7.943	8.498E-01	37.3
10	9.391E-01	40.6
12.59	1.050E+00	43.8
15.85	1.187E+00	46.9
19.95	1.355E+00	49.6
25.12	1.560E+00	52.0

Field Impedance, Stator Open
Test Data

Frequency Hz	Impedance Ohms	Phase Degrees
31.62	1.806E+00	53.9
39.81	2.095E+00	55.2
50.12	2.424E+00	56.2
63.1	2.791E+00	56.8
79.43	3.180E+00	57.3
100	3.578E+00	58.0
125.9	3.960E+00	58.8
158.5	4.298E+00	60.1
199.5	4.554E+00	62.0
251.2	4.691E+00	64.5
316.2	4.675E+00	67.4
398.1	4.497E+00	70.7
501.2	4.173E+00	73.8
631	3.742E+00	76.6
794.3	3.255E+00	78.9
1000	2.767E+00	80.4

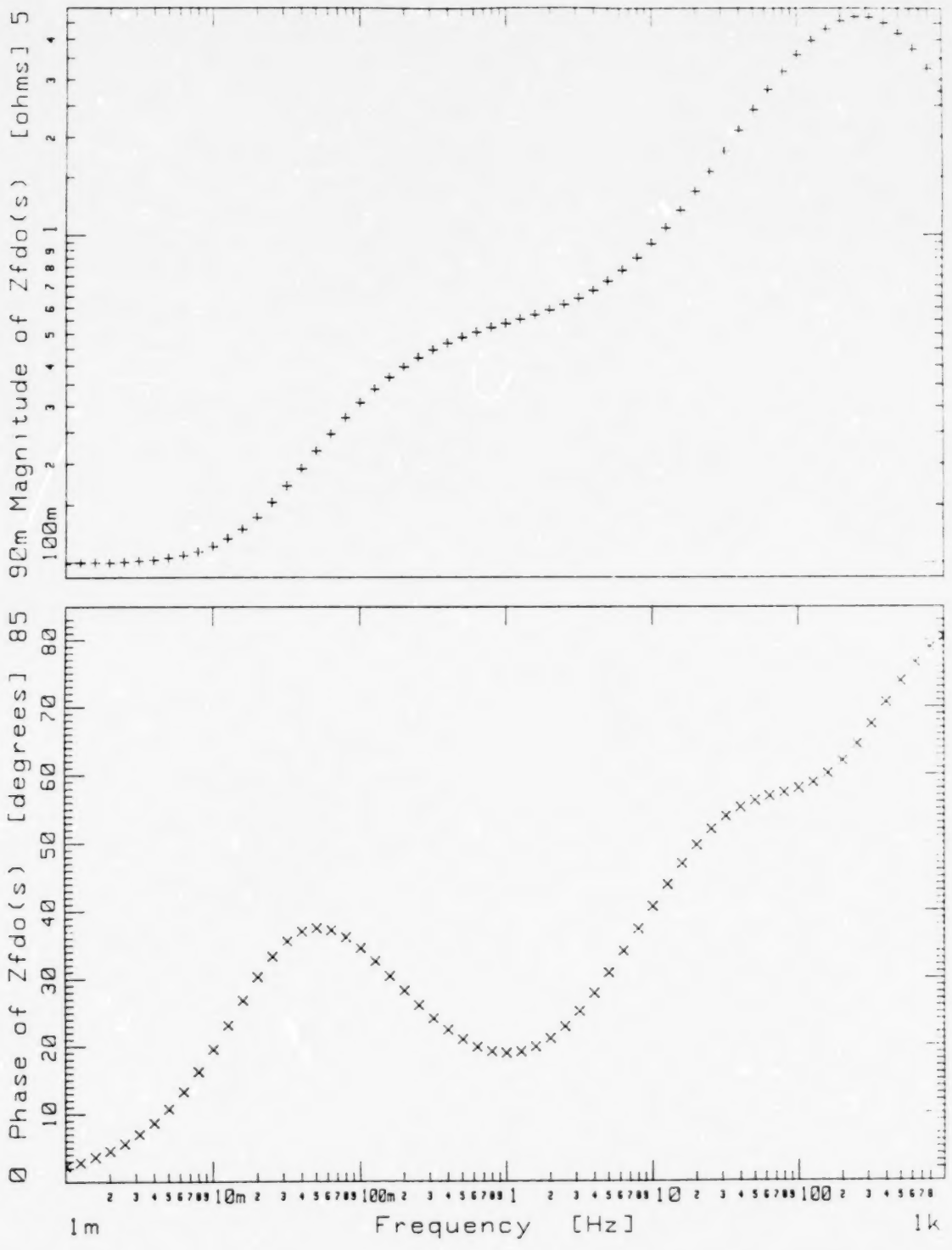

Figure A-10: Field Impedance, Stator Open, $Z_{fdo}(s)$, Magnitude and Phase vs. Frequency

DISTRIBUTION

— Mr. J. S. Edmonds (5)	EPRI	Palo Alto, CA, USA
— Dr. I. M. Canay	Brown Boveri	Baden, Switzerland
— Mr. R. D. Reicker	Brown Boveri	Canada
Mr. P. L. Dandeno	Power Group, Elec. Eng. Dept.	University of Toronto
Mr. L. J. Rubino	System Planning	H04 G25
Dr. P. Kundur / Mr. G. J. Rogers	System Planning	H05 J21
Mr. R. Jeffreys	D & D - Gen	H13 A04
Mr. J. Kapler	D & D - Gen	H13 A06
Mr. Z. J. Janik	D & D - Gen	H15 A14
Mr. W. G. Lobban	D & D - Gen	H15 F18
Mr. C. E. Graham	Power System Op.	A06 A13
Mr. M. E. Coultes	Power System Op.	Richview
Mr. I. Haque	Tech. & Trg. Services	A08 H04
Mr. R. F. Gibson	Station Mgr, Atikokan TGS	Thunder Bay TGS
Mr. C. J. Pyne	Tech. Supt., Atikokan TGS	Thunder Bay TGS
Mr. A. F. Baljet	Electrical Research	KR120
Mr. D. C. Lee	Electrical Research	KR132
Mr. R. E. Beaulieu	Electrical Research	KR132
Mr. J. R. R. Service (2)	Electrical Research	KR132

Public Reference Centre
Editorial Section (2)
Office Copies (2)
Extra Copies